J. Fluid Mech. (2002), *vol.* 459, *pp.* 397–428. © 2002 Cambridge University Press
DOI: 10.1017/S0022112002008157 Printed in the United Kingdom

Second-order integral model for a round turbulent buoyant jet

By HONGWEI WANG AND ADRIAN WING-KEUNG LAW

School of Civil and Environmental Engineering, Nanyang Technological University, Singapore 639798

(Received 20 January 2000 and in revised form 25 September 2001)

The development of a second-order integral model for a round turbulent buoyant jet is reported based on new experimental data on turbulent mass and momentum transport. The mean and turbulent characteristics of a round vertical buoyant jet covering the full range from jets to plumes were investigated using a recently developed combined digital particle image velocimetry (DPIV) and planar laser-induced fluorescence (PLIF) system. The system couples the two well-known techniques to enable synchronized planar measurements of flow velocities and concentrations in a study area. The experimental results conserved the mass and momentum fluxes introduced at the source accurately with closure errors of less than 5%. The momentum flux contributed by turbulence and streamwise pressure gradient was determined to be about 10% of the local mean momentum flux in both jets and plumes. The turbulent mass flux, on the other hand, was measured to be about 7.6% and 15% of the mean mass flux for jets and plumes respectively. While the velocity spread rate was shown to be independent of the flow regime, the concentration-to-velocity width ratio λ varied from 1.23 to 1.04 during the transition from jet to plume. Based on the experimental results, a refined second-order integral model for buoyant jets that achieves the conservation of total mass and momentum fluxes is proposed. The model employs the widely used entrainment assumption with the entrainment coefficient taken to be a function of the local Richardson number. Improved prediction is achieved by taking into account the variation of turbulent mass and momentum fluxes. The variation of turbulent mass flux is modelled as a function of the local Richardson number. The turbulent momentum flux, on the other hand, is treated as a fixed percentage of the local mean momentum flux. In addition, unlike most existing integral models that assume a constant concentration-to-velocity width ratio, the present model adopts a more accurate approach with the ratio expressed as a function of the local Richardson number. As a result, smooth transition of all relevant mean and turbulent characteristics from jet to plume is predicted, which is in line with the underlying physical processes.

1. Introduction

The discharge of waste such as the disposal of wastewater via ocean outfalls or gaseous releases via chimney stacks often leads to the formation of turbulent buoyant jets in the initial dilution stage where the discharge-induced turbulent mixing is the dominant mechanism for the dilution of pollutants in the ambient fluid. Quantifying the entrainment and mixing processes is a key element for both the optimal design of the discharge facilities and the related environmental impact assessment.

https://doi.org/10.1017/S0022112002008157 Published online by Cambridge University Press

Integral models, which are based on the conservation equations of mass, momentum, buoyancy and (where appropriate) species concentration fluxes, are widely used in engineering practice for the prediction of initial dilution for these buoyant jet discharges. Standard references can be found in, for example, Fischer *et al.* (1979). For a round turbulent buoyant jet, numerous experimental investigations have been conducted in the past few decades and the results provided support for the integral modelling approach. Corrsin & Uberoi (1950) reported an early study on the characteristics of a heated turbulent air jet. Recognizing that the measurements by Corrsin & Uberoi might not be far enough downstream to attain self-preservation for the turbulence quantities, Wygnanski & Fiedler (1969) conducted a comprehensive study of the mean velocities and turbulence fluctuations in the truly self-preserving range of a jet with hot-wire anemometer. Their work became a frequent reference for jet studies. However, their measurements showed a significant shortfall in axial momentum flux conservation (Baker 1980; Seif 1981). Capp (1983) and George (1990) attributed this deficiency to the existence of recirculation with a return flow induced by the limited size of the experimental facilities. Panchapakesan & Lumley (1993*a*, *b*) performed a careful examination on a round air jet using a x-wire hot-wire probe mounted on a moving shuttle. The shuttle was used to eliminate errors due to flow reversal in the intermittent region. The turbulent characteristics were analysed to second and third moments and reported in great detail. Hussein, Capp & George (1994) performed a similar examination on an air jet in a much larger facility than Wygnanski & Fiedler (1969) using burst-mode laser Doppler anemometry (LDA), stationary hot-wire (SHW) and flying hot-wire (FHW) probes. The results of LDA and FHW differed substantially from those of SHW (including a thinner velocity width measured by LDA and FHW), raising doubt on the validity of the traditional SHW technique for turbulent jets. Their results were mostly in good agreement with Panchapakesan & Lumley (1993*a*, *b*).

For plumes, the experimental studies reported in the literature are relatively scarce. George, Alpert & Tamanini (1977) measured the velocity and temperature in an air plume simultaneously using a hot-wire probe combined with a cold-wire for temperature detection. They found that the turbulent mass flux constituted about 15% of the total mass flux. The velocity width was determined to be wider than the temperature width, which is contrary to the jet case and also opposite to the findings of Rouse, Yi & Humphrey (1952). All measurements were made at a short distance from the nozzle of 8, 12 and 16 diameters downstream and therefore the assumed self-similarity may not be strictly valid (List 1982). Papanicolaou (1984) pointed out the problem of using temperature as the scalar indictor in plume experiments as the temperature-based methods cannot achieve sufficient accuracy in the far field. He performed a comprehensive experimental study on vertical buoyant jets from jet to fully developed plume regime in water using a combined LDA and laser-induced fluorescence (LIF) technique. The measurements were taken in a region from 20D to 100D, thus extending much further than George *et al.* (1977). The results were reported in Papanicolaou & List (1988). The velocity width obtained for the plume was similar to Rouse *et al.* (1952) but much thinner than George *et al.* (1977). However, their LIF measurements overestimated the mean concentration by up to 20%, which the authors attributed to the absorption of rhodamine on the scattering seeding particles used for LDA. In an attempt to resolve the disagreement among the published plume data, Shabbir & George (1994) carried out another comprehensive experimental study on plumes using two-wire and three-wire probes to simultaneously measure the velocity and temperature. Due to the long experimentation time (a few hours), they made a

https://doi.org/10.1017/S0022112002008157 Published online by Cambridge University Press

special effort to ensure that the ambient air was not self-contaminated and stratified. The results obtained were similar to George *et al.* (1977) but differed substantially from Papanicolaou & List (1988), especially in the velocity spread rate. However, their measurements might be subject to errors associated with SHW, and the fact that the data were taken within a relatively short distance from the source (less than 30D). Good reviews on buoyant jets include Fischer *et al.* (1979), Chen & Rodi (1980) and List (1982).

Most existing integral models consider only the mean mass and momentum fluxes in the set of conservation equations. Hence, they can be referred to as first-order integral models. Although the first-order models give reasonable results for gross prediction, improvement is needed in several areas. First, the contribution of turbulent mass flux is commonly ignored by assuming that it is negligibly small compared to the mean mass flux (e.g. Fischer *et al.* 1979; Noutsopoulos & Yannopoulos 1987; Jones & Baddour 1991). The few models that do account for the contribution treat it as a fixed percentage of the mean value (e.g. Wood, Bell & Wilkinson 1993). In reality, the percentage of turbulent mass flux is not necessarily small and may vary substantially for the buoyant jets in different regimes (momentum-dominated, transitional or buoyancy-dominated) and different environments (cross-flows, waves, etc.). Thus there is a need to quantify the contribution of turbulent mass flux to further improve the prediction. Second, the first-order integral models typically use only the mean momentum flux for total momentum flux conservation. An argument for this assumption is that the momentum flux induced by turbulence is mostly neutralized by the contribution from the streamwise pressure gradient (e.g. Wood *et al.* 1993). However, after the neutralization, the leftover part may still not be negligible and hence refinement is necessary for better quantification. Third, there remains insufficient experimental evidence to confirm a common hypothesis in the first-order models that the width ratio of concentration to velocity is constant from jet to plume. An integral model that incorporates the variation of both mean quantities as well as second-order turbulent quantities such as turbulent mass and momentum fluxes can be termed a second-order integral model due to the improvement in accuracy.

The objective of the present study is to develop a second-order integral model for a vertical round turbulent buoyant jet. To support the development, experiments were conducted to investigate both the mean and turbulent characteristics of the buoyant jet covering the full range from jet-like to plume-like. The experiments adopted a combined digital particle image velocimetry (DPIV) and planar laser-induced fluorescence (PLIF) approach (Law & Wang 2000). In the following sections, the second-order integral model is first derived based on the conservation equations for total mass and momentum fluxes. The newly introduced unknown variables in the model are highlighted. Then the experimental set-up is described and results reported with a comprehensive assessment of the data quality. Finally the set of equations for the second-order integral model are summarized with the variables properly modelled based on the experimental results.

2. Governing equations

For an axisymmetric turbulent buoyant jet within the Boussinesq range, neglecting the molecular diffusion (which is small compared to the turbulent diffusion), the Reynolds-averaged governing equations can be written in cylindrical coordinates (radial direction r, axial direction z, azimuthal direction θ) as

https://doi.org/10.1017/S0022112002008157 Published online by Cambridge University Press

continuity:

$$\frac{1}{r}\frac{\partial r\bar{u}}{\partial r}+\frac{\partial \bar{w}}{\partial z}=0, \tag{1}$$

axial momentum:

$$\bar{u}\frac{\partial \bar{w}}{\partial r}+\bar{w}\frac{\partial \bar{w}}{\partial z}=-\frac{1}{r}\frac{\partial}{\partial r}r\overline{w'u'}-\frac{\partial}{\partial z}(\overline{w'^2}-\overline{u'^2})+g\frac{\overline{\Delta\rho}}{\rho_a}, \tag{2}$$

advection-diffusion:

$$\bar{u}\frac{\partial \bar{c}}{\partial r}+\bar{w}\frac{\partial \bar{c}}{\partial z}=-\frac{1}{r}\frac{\partial r\overline{u'c'}}{\partial r}-\frac{\partial \overline{w'c'}}{\partial z}, \tag{3}$$

where u, w and v are the velocity components in the r-, z- and θ-directions respectively, c the passive scalar concentration, g the gravitational acceleration, ρ_a the ambient fluid density, and $\Delta\rho$ the local density difference with respect to ρ_a. The concentration c in (3) can be replaced by the effective gravitational acceleration Δ $(=(\Delta\rho/\rho_a)g)$ to yield the buoyancy transport equation.

Equation (2) is obtained by approximating the streamwise pressure gradient term in the original Navier–Stokes equation with the term $\partial\overline{u'^2}/\partial z$, i.e. (see e.g. Hussein *et al.* 1994 and Shabbir & George 1994):

$$-\frac{\partial \bar{p}}{\rho_a \partial z}\approx\frac{\partial(\overline{u'^2}+\overline{v'^2})}{2\partial z}\approx\frac{\partial \overline{u'^2}}{\partial z}. \tag{4}$$

According to Hussein *et al.* (1994) and Panchapakesan & Lumley (1993*a*, *b*), the turbulent intensity in the azimuthal direction ($\overline{v'^2}$) is virtually identical to that in the radial direction ($\overline{u'^2}$) for both jets and plumes. Integrating the continuity equation (1) across the buoyant jet yields the relationship between the mean radial and axial velocities:

$$\bar{u}=-\frac{1}{r}\int_0^r\frac{\partial \bar{w}}{\partial z}r\,\mathrm{d}r. \tag{5}$$

With the help of (5), equations (2) and (3) can be integrated over the entire cross-sectional area of the buoyant jet to yield

$$2\pi\frac{\mathrm{d}}{\mathrm{d}z}\int_0^\infty[\bar{w}^2+\overline{w'^2}-\overline{u'^2}]r\,\mathrm{d}r=2\pi\int_0^\infty g\frac{\overline{\Delta\rho}}{\rho_a}r\,\mathrm{d}r, \tag{6}$$

$$2\pi\frac{\mathrm{d}}{\mathrm{d}z}\int_0^\infty(\overline{wc}+\overline{w'c'})r\,\mathrm{d}r=0. \tag{7}$$

Equation (6) is the second-order axial momentum balance equation, with the left-hand side representing the rate of change of total momentum flux with respect to z and the right-hand side being the local buoyancy flux. The total momentum flux ($M=M_M+M_{TP}$) here has already incorporated the turbulent momentum flux and the contribution of streamwise pressure gradient (we use M_{TP} to represent the sum of the two), which are of second-order magnitude compared with the mean momentum flux (M_M). The following equations are used to compute M_M and M_{TP}:

$$M_M=2\pi\int_0^\infty\bar{w}^2r\,\mathrm{d}r, \tag{8}$$

$$M_{TP}=2\pi\int_0^\infty[\overline{w'^2}-\overline{u'^2}]r\,\mathrm{d}r. \tag{9}$$

https://doi.org/10.1017/S0022112002008157 Published online by Cambridge University Press

Equation (7) is the second-order mass flux conservation equation which dictates that the total mass flux ($H = H_M + H_T$) should be conserved in a buoyant jet. The mean and turbulent mass fluxes, H_M and H_T, are defined by

$$H_M = 2\pi \int_0^\infty \overline{w}\overline{c} r \, \mathrm{d}r, \tag{10}$$

$$H_T = 2\pi \int_0^\infty \overline{w'c'} r \, \mathrm{d}r. \tag{11}$$

To account for the turbulent momentum and mass fluxes in the integral model, we define two variables, k_M and k_H, as the ratios of total flux to mean flux for momentum and mass respectively:

$$k_M = 1 + \frac{M_{TP}}{M_M}, \tag{12}$$

$$k_H = 1 + \frac{H_T}{H_M}. \tag{13}$$

It is well known that the cross-sectional profiles of normalized mean axial velocity and concentration are Gaussian-like in the zone of established flow (ZEF), i.e.

$$\frac{\bar{w}}{\overline{w}_c} = \exp\left[-\left(\frac{r}{\eta_w z}\right)^2\right], \tag{14}$$

$$\frac{\bar{c}}{\overline{c}_c} = \exp\left[-\left(\frac{r}{\eta_c z}\right)^2\right], \tag{15}$$

where the subscript c denotes the centreline value of the respective quantity, η_w the velocity spread rate or dimensionless velocity 1/e width, and η_c the concentration spread rate or dimensionless concentration 1/e width. We define λ as the concentration-to-velocity width ratio, i.e.

$$\lambda = \eta_c / \eta_w. \tag{16}$$

It should be noted that η_w, η_c and λ are not necessarily constant as the buoyant jet evolves from jet-like to plume-like. Equation (15) can also be used to describe the cross-sectional distribution of the effective gravitational acceleration Δ ($= (\Delta\rho/\rho_a)g$) if c is replaced by Δ.

With the above Gaussian assumption and the variables k_M, k_H and λ, (6) and (7) can be integrated over the cross-sectional area to yield the conservation equations for momentum and buoyancy fluxes respectively:

$$\frac{\mathrm{d}M}{\mathrm{d}z} = \frac{\mathrm{d}}{\mathrm{d}z}\left(k_M \frac{\pi}{2} \bar{w}_c^2 \eta_w^2 z^2\right) = \pi \overline{\Delta}_c \lambda^2 \eta_w^2 z^2, \tag{17}$$

$$\frac{\mathrm{d}B}{\mathrm{d}z} = \frac{\mathrm{d}}{\mathrm{d}z}\left(k_H \frac{\lambda^2}{1+\lambda^2} \pi \overline{w}_c \overline{\Delta}_c \eta_w^2 z^2\right) = 0, \tag{18}$$

where B is the total buoyancy flux. There are six unknowns in the above two equations for a given z: k_M, k_H, λ, η_w, $\overline{w}_c$ and $\overline{\Delta}_c$. To solve the equations, most first-order integral models make the following two simplifications: (i) the turbulent momentum and mass fluxes are ignored by assuming that k_M and k_H are equal to 1, and (ii) the concentration-to-velocity width ratio λ is assumed to be a constant, and usually the value of the plume width ratio λ_p is adopted since any buoyant jet will

https://doi.org/10.1017/S0022112002008157 Published online by Cambridge University Press

eventually become plume-like. This is despite the fact that some previous experiments (e.g. Papanicolaou & List 1988) have shown that λ actually varies from jet to plume. With the above simplifications, the number of unknowns reduces to three, η_w, $\overline{w_c}$ and $\overline{\Delta_c}$. Either a constant velocity spread rate assumption (i.e. η_w = constant) (e.g. Wood *et al.* 1993) or an entrainment assumption (e.g. Fischer *et al.* 1979) can then be used to close the set of conservation equations. The two closure assumptions are related as Jirka & Harleman (1979) were able to derive the entrainment function based on the constant velocity spread rate assumption (see also Wood *et al.* 1993).

The entrainment hypothesis was made by Morton, Taylor & Turner (1956) as

$$\frac{\mathrm{d}Q}{\mathrm{d}z} = \frac{\mathrm{d}}{\mathrm{d}z}(\pi \bar{w}_c \eta_w^2 z^2) = 2\pi\alpha\eta_w z \bar{w}_c, \tag{19}$$

where Q is the volume flux and α the entrainment coefficient. Previous experiments have shown that the entrainment coefficients for jets and plumes differ. List (1982) summarized much of the work on the entrainment hypothesis and proposed values of $\alpha_j = 0.0535$ for jets and $\alpha_p = 0.0833$ for plumes. The entrainment coefficient varies from α_j to α_p during the transition from jet-like to plume-like. To model this variation, two types of formulation are commonly used in the existing integral models. One was derived based on the conservation of energy by Priestley & Ball (1955) as

$$\alpha = \alpha_j - (\alpha_j - \alpha_p)\left(\frac{R}{R_p}\right)^2. \tag{20}$$

The other is an empirical function proposed by List (1982):

$$\alpha = \alpha_j \exp\left[\ln\left(\frac{\alpha_p}{\alpha_j}\right)\left(\frac{R}{R_p}\right)^2\right]. \tag{21}$$

In the above two equations, R is the local Richardson number defined as

$$R = \frac{QB^{1/2}}{M^{5/4}} \tag{22}$$

that represents the ratio of buoyancy to inertial force. It varies from 0 in jets to a constant value (R_p) in plumes. Both (20) and (21) are essentially different types of interpolation between the entrainment coefficients for jets and plumes that satisfy the two asymptotic cases.

For the closure of the second-order integral model, an additional three unknowns, k_M, k_H and λ, must be solved. Although experimental data for their values in jets and plumes have been reported before (e.g. Papanicolaou & List 1988), there remains a lack of quantitative description of how they vary during the transition from jet-like to plume-like. In the following, we describe a series of experiments on a round buoyant jet with a specific focus on quantifying the transitional behaviour.

3. Experimental set-up

A schematic diagram of the experimental set-up is shown in figure 1. The experiments were conducted in a 3 m(L) × 1 m(W) × 1 m(H) glass test tank filled with fresh tap water to a depth of 0.9 m. The sidewalls and bottom wall were made of 15 mm thick clear glass. A buoyant jet of salt water was driven by a constant-head tank and discharged from a round port made from a stainless steel hollow tube into the ambient fresh water. The constant-head tank generated a very consistent discharge

https://doi.org/10.1017/S0022112002008157 Published online by Cambridge University Press

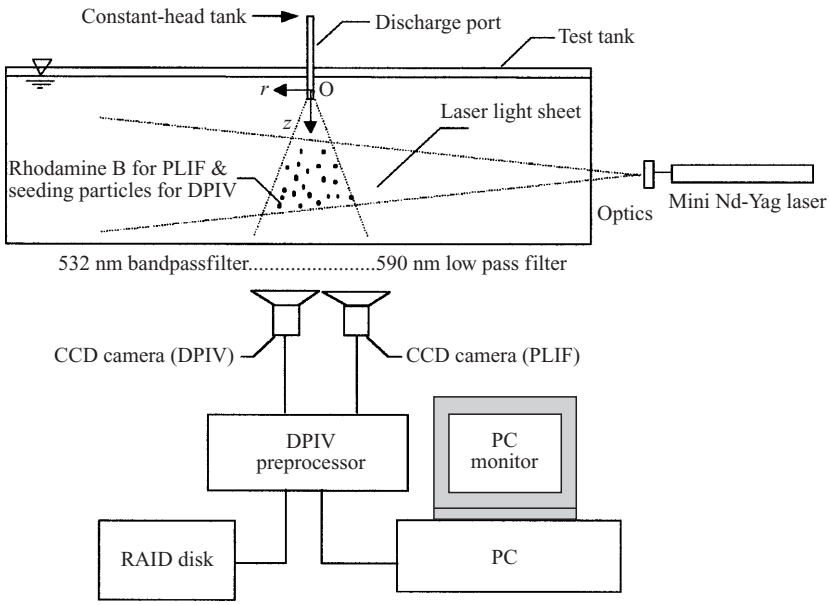


FIGURE 1. Experimental set-up for buoyant jet investigations using combined PIV and PLIF.

flow rate, which was adjustable through a valve and monitored by a rotameter. The flow rate for each experiment was calibrated using a precision measuring cylinder and a stopwatch. The steel hollow tube was about 0.3 m long, which should generate a fully developed pipe flow with no swirl at the exit. The tube was located at a position of 0.6 m from a side panel along the longitudinal centreline of the tank in consideration of the diffuse angle of the laser light sheet and the PLIF sensitivity. The submergence of the discharge port was approximately 0.05 m. The temperature variation from the source to the imaging window was measured to be less than 0.2 °C. Thus the ambient fluid was essentially non-stratified. Water temperature in the test tank and constant-head tank was maintained to be approximately 25 °C, avoiding the effect of temperature fluctuation on the fluorescence efficiency of the dye tracer. The laboratory was kept dark during the experiments in order to minimize the possible impact on PLIF due to ambient light.

The velocity and concentration measurements were based on a combined DPIV/PLIF approach (Law & Wang 2000). Here only a brief summary of the approach is given. The light source employed was a dual-cavity pulsed mini Nd:YAG laser with a maximum repetition rate of 15 Hz for each cavity. The energy level was 25 mJ per pulse and the pulse duration was about 7 ns. The emitted laser light was green with a wavelength of 532 nm. The light sheet had a typical thickness of 3 mm and a divergence angle of 32°. Two double-image 8-bit digital CCD cameras (Kodak Megaplus ES1.0) were configured, one for DPIV and the other for PLIF. The spatial resolution of the cameras was 1008×1018 pixels. Both cameras were fitted with a Nikon 60 mm lens. The PLIF camera was set to single-frame mode while the DPIV camera worked in double-frame mode. Thus the PLIF image was double-exposed by the laser pulse pair, the interval of which was determined by the cross-correlation DPIV requirement. The double exposure improved the PLIF sensitivity. The timing diagram for the laser and camera synchronization was set in such a manner that both the measured velocity and concentration were time-mean values during the pulse pair

https://doi.org/10.1017/S0022112002008157 Published online by Cambridge University Press

interval. The two cameras were pointed to nearly the same area with a typical size of 18 cm × 18 cm. The overlapped area of the two imaging windows was determined through spatial reference points during calibration.

Neutrally buoyant polyamid particles with a density of $1.03 \times 10^3\,\mathrm{kg\,m^{-3}}$ and mean diameter of 50 mm were chosen as the seeding particles for DPIV. Following Mei (1996), the error resulting from the density discrepancy between the seeding particles and water was calculated to be less than 3% at 1 kHz. The error should be further reduced at the relatively lower energy-containing frequency of the turbulent fluctuations in jets and plumes.

Rhodamine B was selected as the fluorescent dye tracer for PLIF. According to Berlman (1971), the absorption spectrum of Rhodamine B is from 460 to 590 nm with a peak at 550 nm, while its emission spectrum ranges from 550 nm to 680 nm with a peak at 590 nm. An optical 532 nm band-pass filter was placed in front of the DPIV camera, allowing only a narrow band of wavelengths around 532 nm scattered by the seeding particles to pass through. Another optical 590 nm sharp-cut low-pass filter was attached to the PLIF camera, allowing through only the fluorescent light emitted from the dye tracer.

The system was capable of recording the DPIV image pairs and PLIF image at a frequency up to 7 Hz for a few minutes. The relatively long measuring duration was made possible by employing a RAID cabinet as an intermediate transfer buffer before the images were slowly processed and written to the hard disk.

In the core of the buoyant jets, a spatial variation of refractive index existed due to the varying salinity. This index variation can potentially lead to the distortion of the captured images and hence measurement errors. However, the refractive error was found to be negligible in the present experiments due to the small density difference and slender jet width in the measured area.

An inherent limitation in combining DPIV and PLIF is that the spatial PLIF resolution in the direction perpendicular to the laser sheet is relatively low. This is because DPIV requires a certain thickness of the laser light sheet to prevent seeding particles from moving out of plane during the pulse pair interval that may otherwise lead to a significant bias in the velocity determination. The thickness of the light sheet would induce a slight spatial smearing of the measured concentrations and velocities. However, the error can be greatly reduced or even ignored by taking measurements in an area sufficiently far from the discharge port with the flow dimension much larger than the light sheet thickness.

Various experiments were carried out to quantify the characteristics of different parts of the system. Further details of the verification experiments and the calibration procedures as well as a discussion of this combined approach can be found in Wang (2000).

The measurements were initiated just after the jet flow became steady in the clear ambient water. The typical sampling rate was 5 Hz and the duration of sampling was 60 s. The relatively short duration avoided self-contamination and accumulation of dye and seeding particles in the region between the laser source and the image area caused by the re-circulation within the confinement of the tank, which would otherwise significantly attenuate the laser light and affect the PLIF readings. The adopted sampling duration should be adequate for statistical turbulence analysis, as it is much longer than the large-scale times (using the formula suggested by Papanicolaou & List 1989) estimated to be 0.8 s and 2.8 s for the jets and plumes respectively in this study.

The combined DPIV and PLIF set-up can be used to determine the mean charac-

https://doi.org/10.1017/S0022112002008157 Published online by Cambridge University Press

Exp.	r range of image (mm)	z range of image (mm)	w_0 (m s^{-1})	D (mm)	$\Delta\rho_0/\rho_a$ (%)	Re	L_m (mm)
PSDAJ1 (D)	−36.0–36.9	−8.7–64.9	0.570	9.4	0	6000	∞
PSDAJ2 (D)	−35.8–37.8	64.4–138.7	0.570	9.4	0	6000	∞
PSDAJ3 (D)	−36.2–37.5	138.1–212.5	0.570	9.4	0	6000	∞
PSDAJ4 (D)	−35.8–38.8	211.8–287.1	0.570	9.4	0	6000	∞
PSDAJ5 (D)	−58.2–61.8	285.8–407.0	0.570	9.4	0	6000	∞
PSPAJ1 (P)	−111.3–112.5	−4.2–221.8	0.570	9.4	0	6000	∞
PSPAJ2 (P)	−115–108.6	123.2–349.0	0.570	9.4	0	6000	∞
PSDPAJ1 (D)	−84.8–79.3	177.8–343.5	2.520	4.5	0	12700	∞
(P)	−94.3–87.0	166.9–350.0					
BSDPAJ2 (D)	−114.2–112.5	299.8–70.9	1.823	4.5	1.17	9190	340
(P)	−127.6–112.4	308.0–65.6					
BSDPAJ4 (D)	−114.2–112.5	299.8–70.9	1.258	4.5	2.88	6340	149
(P)	−127.6–112.4	308.0–65.6					
BSDPAJ5 (D)	−114.2–112.5	299.8–70.9	1.886	4.5	2.88	9510	224
(P)	−127.6–112.4	308.0–65.6					
BSDPAJ6 (D)	−116.0–111.4	297.0–67.3	0.173	9.4	2.84	1820	30
(P)	−129.4–111.1	305.6–62.7					
BSDPAJ7 (D)	−116.0–111.4	297.0–67.3	0.432	9.4	2.84	4550	75
(P)	−129.4–111.1	305.6–62.7					
BSDPAJ8 (D)	−106.5–105.4	506.0–292	1.006	4.5	2.84	5070	120
(P)	−115.2–106.8	513.8–289.6					
BSDPAJ9 (D)	−106.5–105.4	506.0–292	1.886	4.5	2.84	9510	226
(P)	−115.2–106.8	513.8–289.6					
BSDPAJ10 (D)	−109.5–102.5	505.0–290.9	0.147	9.4	2.84	1550	25
(P)	−117.8–104.8	511.7–286.9					
BSDPAJ11 (D)	−109.5–102.5	505.0–290.9	0.403	9.4	2.84	4250	70
(P)	−117.8–104.8	511.7–286.9					
BSDPAJ12 (D)	−109.5–102.5	505.0–290.9	0.288	9.4	2.84	3030	50
(P)	−117.8–104.8	511.7–286.9					

TABLE 1. Initial parameters of buoyant jet experiments: (D) denotes DPIV measurement and (P) PLIF.

teristics and the second-order turbulence correlations for jets and plumes, in which most of the turbulence energy is contained by low-frequency and large-scale eddies. This was demonstrated by Papanicolaou & List (1988) who showed that the turbulent energy production occurs primarily in the range 0.1–1 Hz, and from 0.1 to 3 Hz the spectral turbulent energy decreases over two orders of magnitude. However, the ability of the set-up to resolve details at higher frequencies is rather poor, being handicapped by the maximum measurement frequency of only 7 Hz. Furthermore, the spatial velocity resolution in the light sheet plane is rather coarse at 5.7 mm based on interrogation areas of 32×32 pixels with 50% overlapping. This resolution is larger than the Komogorov length scale in the range of 0.1–1.0 mm in the study area. Hence, despite the fact that the mean and second-order quantity determination is satisfactory, comprehensive analysis for the turbulence spectrum or dissipation cannot be performed.

The parameters of the different experiments are listed in table 1, where D is the port diameter, w_0 the initial discharge velocity, $\Delta\rho_0$ the initial density difference, and L_m the characteristic length scale defined as (Fischer *et al.* 1979)

$$L_m = M_0^{3/4}/B_0^{1/2}, \tag{23}$$

https://doi.org/10.1017/S0022112002008157 Published online by Cambridge University Press

where M_0 and B_0 are the initial momentum and buoyancy fluxes respectively. In Exps. PSDAJ1–5, only DPIV was conducted while in Exps. PSPAJ1–2, only PLIF was performed. All the other experiments were measured by combining DPIV and PLIF.

4. Experimental results

Exps. PSDAJ1–PSDAJ5, PSPAJ1–PSPAJ2 and PSDPAJ1 covered a dimensionless area from the jet exit to $z/D = 80$ in a pure jet. The experimental data show that both the mean and turbulent characteristics become self-similar beyond $z/D = 25$, which is in agreement with earlier investigations. Exps. BSDPAJ2–BSDPAJ12 were performed in the jet-like, transitional and plume-like regions in a buoyant jet. The measurements covered a dimensionless length z/L_m ranging from 0.2 to 20. The results for a fully developed self-preserving jet (Exp. PSDPAJ1) and plume (Exp. BSDPAJ10) are presented as representative of jets and plumes respectively. The data for Exp. BSDPAJ10 were taken in the region $11.5 < z/L_m < 20$ which, according to Papanicolaou & List (1988), is in the asymptotic plume region.

The data relevant to the second-order integral modelling are presented in the following. Only those data that were acquired in the fully developed region (beyond $z/D = 25$) are reported. It should be noted that most of the experimental results are similar to earlier studies. However, they are still briefly presented here to provide verification for the curve-fitting as well as to lend support to the new data on turbulent mass transport.

4.1. *Mean and turbulent characteristics of velocity*

The centreline mean axial velocity decay in a jet and plume can be described respectively as (e.g. Papanicolaou & List 1988)

jet:

$$\frac{w_0}{\overline{w_c}} = \frac{1}{k_{jw}} \frac{z}{D}, \tag{24}$$

plume:

$$\frac{\sqrt{M_0}}{z\overline{w_c}} = \frac{1}{k_{pw}} \left(\frac{z}{L_m} \right)^{-2/3}, \tag{25}$$

or equivalently:

$$\overline{w_c} = k_{pw} B_0^{1/3} z^{-1/3}. \tag{26}$$

The subscripts 0 and c denote the initial and centreline values respectively. Applying best-fitting to the experimental data yields the decay constants $k_{jw} = 6.48$ for jets and $k_{pw} = 4.13$ for plumes. In this work, a preceding character j in a subscript denotes a quantity for jets and p for plumes whereas a subscript without a preceding character j or p represents the variable for buoyant jets. The value of k_{jw} is in good agreement with 6.2 suggested by Fischer *et al.* (1979) and Chen & Rodi (1980) and 6.71 by Papanicolaou & List (1988), while slightly higher than 6.06 by Panchapakesan & Lumley (1993 and 5.8 by Hussein *et al.* (1994). The value of k_{pw} is close to 3.85 measured by Papanicolaou & List (1988) and 3.79 proposed by Chen & Rodi (1980), but lower than 4.7 by Rouse *et al.* (1952) and Fischer *et al.* (1979), while substantially higher than 3.4 by George *et al.* (1977) and Shabbir & George (1994). Comparison of the jet and plume constants reported in different studies are tabulated in tables 2 and 3 respectively.

https://doi.org/10.1017/S0022112002008157 Published online by Cambridge University Press

	k_{jw}	η_{jw}	k_{jc}	η_{jc}	$\frac{\sqrt{\overline{w_c'^2}}}{\overline{w_c}}$	$\frac{\sqrt{\overline{u_c'^2}}}{\overline{w_c}}$	$\frac{\sqrt{\overline{c_c'^2}}}{\overline{c_c}}$	z/D	Re
Present study	6.48	0.106	5.26	0.129	0.27	0.19	0.224	40–80	12700
Papanicolaou & List (1988)	6.71	0.104	5.37	0.126	0.25	0.17	0.22	40–110	2460–10900
Panchapakesan & Lumley (1993*a*, *b*)	6.06	0.115	—	—	0.24	0.185	—	30–160	11000
Hussein *et al.* (1994)	5.8	0.106	—	—	0.276	0.218	—	15–100	95500
Dahm & Dimotakis (1990)	—	—	5.4	—	—	—	0.225	0–350	5000
Fischer *et al.* (1979)	6.2	0.107	4.96	0.127	—	—	—	—	—
Chen & Rodi (1980)	6.2	0.103	5.0	0.136	—	—	—	—	—

TABLE 2. Comparison of jet characteristics reported in different studies. Note that the original cross-sectional distribution of mean axial velocity reported by Hussein *et al.* (1994) is $\bar{w}/\overline{w_c} = \exp -78.4(r/(z-4D))^2]$. Since it was obtained by curve-fitting of the experimental data (LDA) at $z/D = 70$, it can be converted to the format of $\bar{w}/\overline{w_c} = \exp[-(r/0.106z)^2]$ for comparison. Also k_{jc}, k_{pc} and η_{jc} in Papanicolaou & List (1988) are quoted from their previous temperature measurements rather than their LIF results.

	k_{pw}	η_{pw}	k_{pc}	η_{pc}	$\frac{\sqrt{\overline{w_c'^2}}}{\overline{w_c}}$	$\frac{\sqrt{\overline{u_c'^2}}}{\overline{w_c}}$	$\frac{\sqrt{\overline{c_c'^2}}}{\overline{c_c}}$	z/L_m	z/D	$\Delta\rho_0/\rho_a$
Present study	4.13	0.105	11.3	0.109	0.26	0.19	0.42	11.5–20	31–55	$< 3\%$
Papanicolaou & List (1988)	3.85	0.105	11.1	0.112	0.23	0.15	0.39	5–80	22–80	$< 3\%$
Shabbir & George (1994)	3.4	0.131	9.4	0.121	0.32	0.19	0.40	6.5–16	10–28	48%
George *et al.* (1977)	3.4	0.135	9.1	0.124	0.28	—	0.38	7–14	< 16	48%
Rouse *et al.* (1952)	4.7	0.102	11	0.119	—	—	—	—	< 11	—
Fischer *et al.* (1979)	4.7	0.100	9.1	0.120	—	—	—	—	—	—
Chen & Rodi (1980)	3.79	0.135	11	0.125	—	—	—	—	—	—

TABLE 3. Comparison of plume characteristics reported in different studies. See table 2 caption for note regarding Papanicolaou & List data.

The mean axial velocity decay along the centreline is plotted in figure 2. The figure clearly shows that for $z/L_m < 0.6$, the flow is jet-like, and for $z/L_m > 6$, the flow is plume-like. This agrees extremely well with Papanicolaou & List (1988) ($z/L_m < 1$ for jet-like and $z/L_m > 5$ for plume-like) and Chen & Rodi (1980) ($z/L_m < 0.53$ for jet-like and $z/L_m > 5.3$ for plume-like). The pure jet data points cannot be put directly into this log-log plot. A horizontal dotted line is thus used to represent their best-fit line. It can be seen that the decay rate of a buoyant jet in the jet-like region coincides with the one measured in a pure jet.

The smooth solid curve in figure 2 is obtained by applying curve fitting in the following form to the data points:

$$g(\xi) = -\tfrac{1}{3}[1+\tanh(k_1\xi-\eta_1)]\xi + \log\left(\frac{1}{k_{pw}}\right) + \frac{1}{2}\left[\log\left(\frac{1}{k_{pw}}\right) - \log\left(\frac{\sqrt{\pi}}{2k_{jw}}\right)\right][\tanh(k_2\xi-\eta_2)-1] - k_4\exp[-k_3(\xi-\eta_3)^2], \tag{27}$$

https://doi.org/10.1017/S0022112002008157 Published online by Cambridge University Press

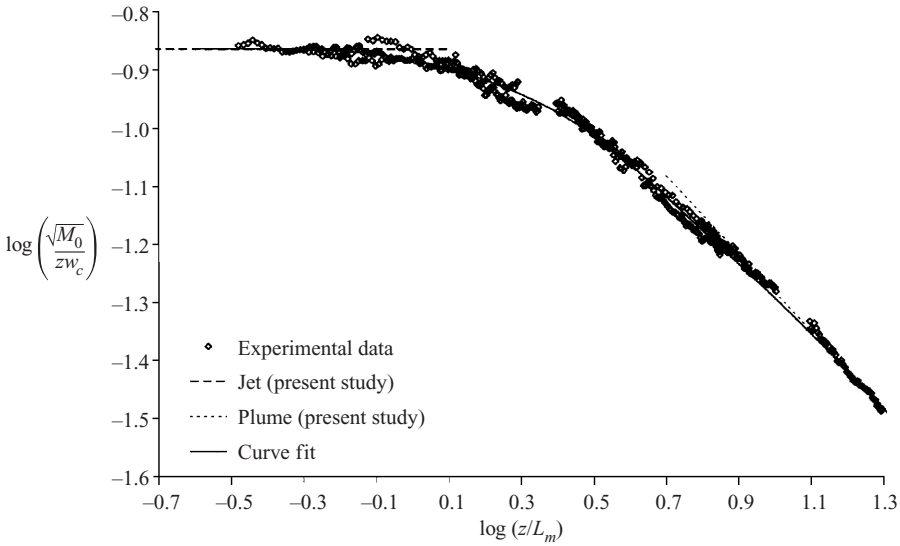


FIGURE 2. Centreline decay of the mean axial velocity in buoyant jets.

where

$$\log\left(\frac{\sqrt{M_0}}{z\overline{w}_c}\right) = g(\xi), \tag{28}$$

$$\xi = \log\left(\frac{z}{L_m}\right). \tag{29}$$

The constants in (27) are determined by the least-square method as: $k_1 = 3.110$, $k_2 = 2.815$, $k_3 = 6.123$, $k_4 = 0.0797$, $\eta_1 = 1.831$, $\eta_2 = 2.067$ and $\eta_3 = 0.4529$. The $k_{jw} = 6.48$ and $k_{pw} = 4.13$ (obtained in this study) are used in the curve-fitting. Equation (27) automatically satisfies the two asymptotic cases of buoyant jets, i.e. pure jets and plumes. The Gaussian function (the last term in (27)) helps to make the curve smoother and match closer the experimental data.

The normalized cross-sectional profiles of mean axial velocity for jets and plumes collapse onto the respective Gaussian curves given by (14) and (15) exceptionally well. Again curve-fitting yields the velocity spread rate (or dimensionless 1/e velocity width): $\eta_{jw} = 0.106$ for jets and $\eta_{pw} = 0.105$ for plumes. It can be seen from table 2 that the measured jet velocity width agrees very well with all other studies except being slightly thinner than that recorded by Panchapakesan & Lumley (1993*a*, *b*). On the other hand, the plume velocity width, while agreeing with Rouse *et al.* (1952), Fischer *et al.* (1979) and Papanicolaou & List (1988), is however about 30% thinner than that reported by George *et al.* (1977), Chen & Rodi (1980), and Shabbir & George (1994). From table 3, we note that a major difference among the experimental parameters of George *et al.* (1977), Shabbir & George (1994) and the present study is the initial density difference. The former two adopted a very high initial density difference of about 48% whereas a value of 2.84% was used here. Obviously, the Boussinesq approximation cannot be applied to the near field of the former two cases and, as a result, the temperature field may not be dynamically passive. Chen & Rodi (1980) reviewed the existing experimental data on buoyant jets. They noted the effect of large initial density difference on the behaviour of buoyant jets and took into account the effect by adding a factor of the initial density ratio in the

https://doi.org/10.1017/S0022112002008157 Published online by Cambridge University Press

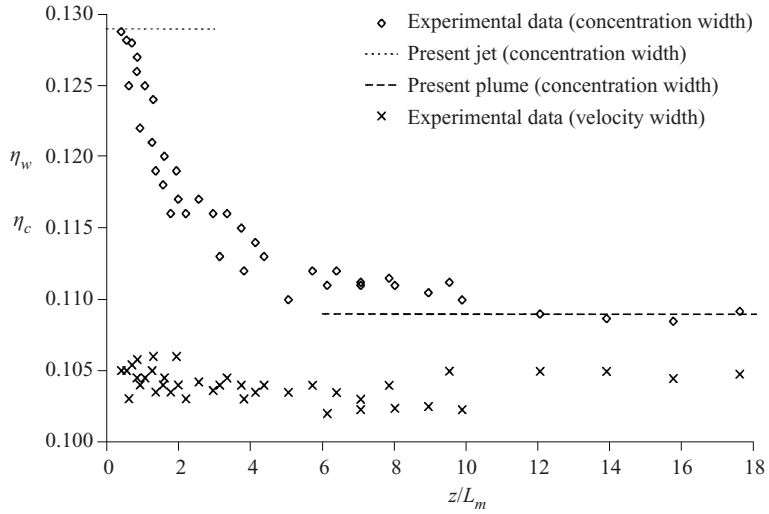


FIGURE 3. Variation of the velocity and concentration width with z/L_m in buoyant jets.

formulation of plume centreline velocity and concentration. We also note that the plume studied here is a water plume in contrast to the air plume measured by George *et al.* (1977) and Shabbir & George (1994). The Schmidt number in water is a few hundred times higher than that in air due to the lower molecular diffusion in water. The effect of Schmidt number on turbulent mixing is generally ignored when the overall mixing is of interest, as molecular diffusion is thought to be small compared to the turbulent diffusion. However, noticeable effects have been reported by some experimental turbulent mixing studies. For example, Dahm & Dimotakis (1990) found that pure ambient fluid was present at a water jet centreline with a probability of up to 30% whereas no such unmixed fluid was found in a comparable air jet. Furthermore, unlike the present plume measurements that were taken in the region $z/D = 31$–55, the experiments of Shabbir & George (1994) were performed in the region $z/D = 10$–28 where the turbulent flow might not be exactly fully developed.

The variation of the dimensionless velocity width η_w during the transition from jet-like to plume-like was measured to be within 3% (see figure 3), implying that the velocity width is essentially constant during the transition. This validates the widely accepted assumption that the rate of velocity expansion of buoyant jets is independent of the type of flow (jet-like or plume-like) that is commonly employed in the integral models as a closure equation (e.g. Abraham 1963; List & Imberger 1973; Jirka & Harleman 1979; Wood *et al.* 1993; etc.). Peterson & Bayazitoglu (1992) performed buoyant jet experiments in the transitional region with LDA. Their measurements also confirmed this assumption.

The centreline velocity fluctuations in the axial and radial directions, $\sqrt{\overline{w_c'^2}}/\overline{w_c}$ and $\sqrt{\overline{u_c'^2}}/\overline{w_c}$, were recorded to be about 27% and 19% for jets, and 26% and 19% for plumes respectively, and are within the range reported in the literature. The cross-sectional variations of turbulent normal and shear stresses, $\sqrt{\overline{w'^2}}/\overline{w_c}$, $\sqrt{\overline{u'^2}}/\overline{w_c}$ and $\overline{w'u'}/\overline{w_c}^2$, for jets and plumes are plotted in figures 4–6. The profiles of $\overline{w'u'}/\overline{w_c}^2$ have a peak value of approximately 0.020 at $r/z \approx 0.62$ for jets and 0.021 at $r/z \approx 0.68$ for plumes. As a comparison, a peak value of 0.018 for jets was recorded by Panchapakesan & Lumley (1993*a*, *b*), 0.021 for jets by Hussein *et al.* (1994), 0.026

https://doi.org/10.1017/S0022112002008157 Published online by Cambridge University Press

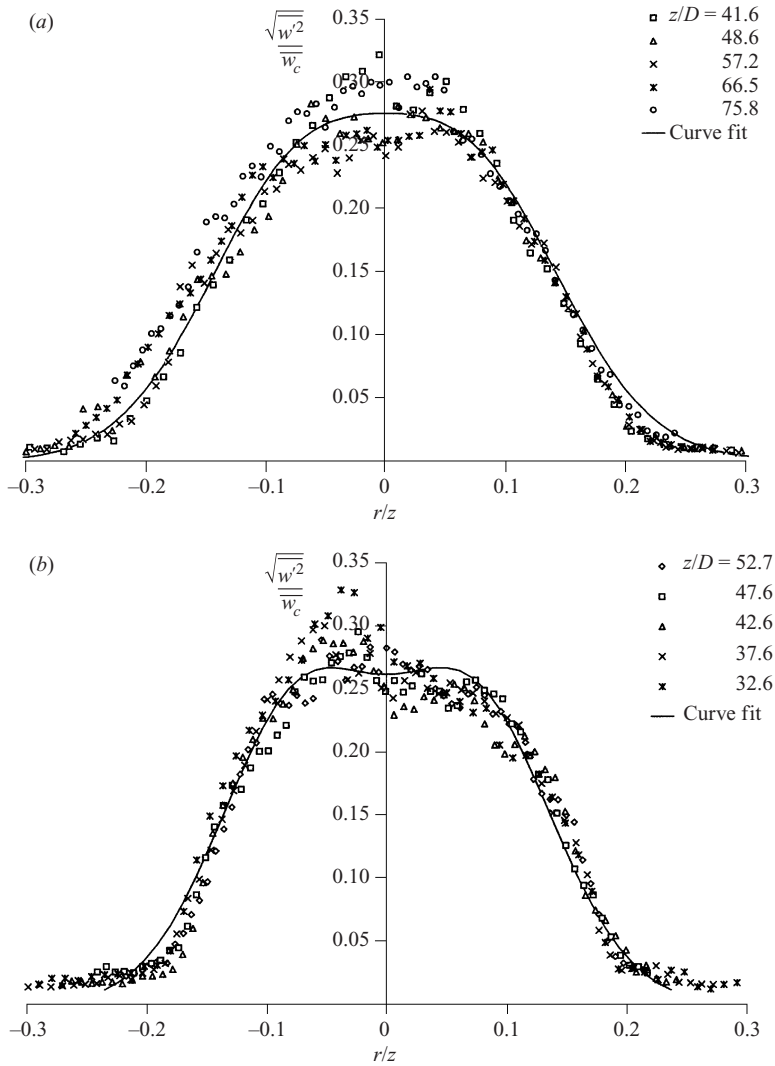


FIGURE 4. Cross-sectional variation of turbulent intensity of the axial velocity in (*a*) jets and (*b*) plumes.

for plumes by Shabbir & George (1994), and much lower values of 0.012 for jets and 0.013 for plumes by Papanicolaou (1984). These figures show that there is actually no distinct difference in the turbulent normal and shear stresses between jets and plumes, which implies that buoyancy has no direct effect on turbulence velocity fluctuations. The buoyancy affects the plume behaviour mainly through the mean velocity. This observation is consistent with George *et al.* (1977), Papanicolaou & List (1988), and Shabbir & George (1994). It is also supported by the experimental data in the fully developed transitional region of the present study.

4.2. *Mean and turbulent characteristics of concentration*

The centreline mean concentration decay in a jet and plume can be described respectively as (e.g. Papanicolaou & List 1988)

https://doi.org/10.1017/S0022112002008157 Published online by Cambridge University Press

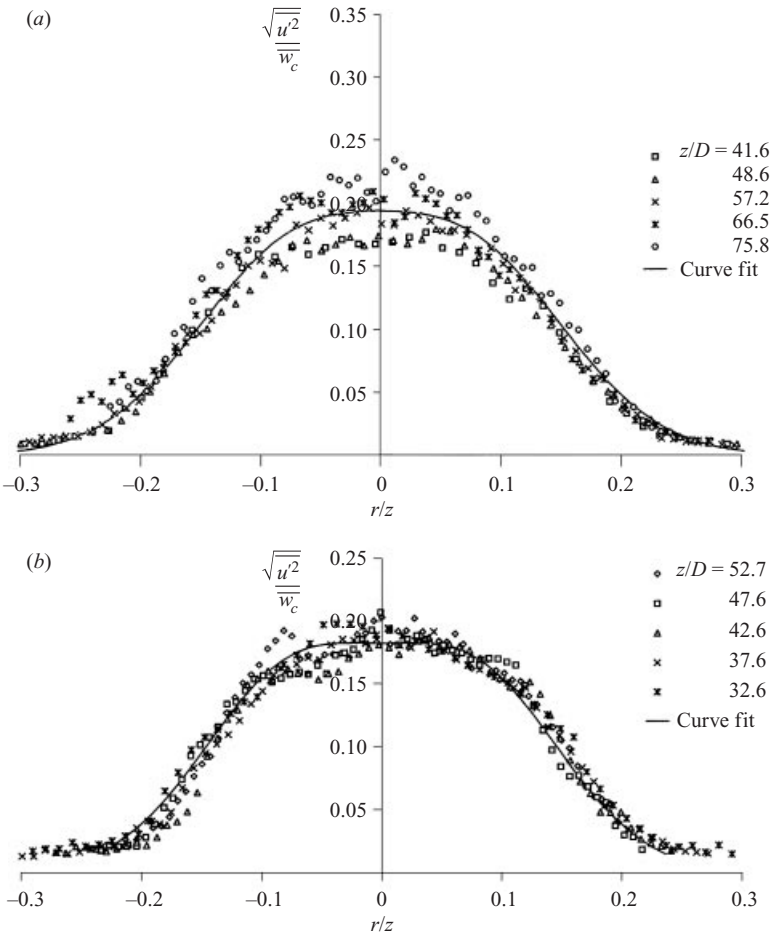


FIGURE 5. Cross-sectional variation of turbulent intensity of the radial velocity in (*a*) jets and (*b*) plumes.

jet:

$$\frac{c_0}{\overline{c_c}} = \frac{1}{k_{jc}}\frac{z}{D}, \tag{30}$$

plume:

$$\frac{C_0 Q_0}{z\overline{c_c}\sqrt{M_0}} = \frac{1}{k_{pc}}\left(\frac{z}{L_m}\right)^{2/3}. \tag{31}$$

Replacing c with Δ in (31) yields the centreline buoyancy decay equation:

$$\overline{\Delta_c} = k_{pc} B_0^{2/3} z^{-5/3}. \tag{32}$$

Again curve fitting to the experimental data yields $k_{jc} = 5.26$ and $k_{pc} = 11.3$. The corresponding best-fit lines are shown in figure 7. The value of k_{jc} compares well with 5.4 by Dahm & Dimotakis (1990), 5.37 by Papanicolaou & List (1988), 4.96 by Fischer *et al.* (1979) and 5.0 by Chen & Rodi (1980). For k_{pc}, there exists some disagreement among the existing data. A value of 11 was reported by Rouse *et al.* (1952) and Chen & Rodi (1980), and 11.1 by Papanicolaou & List (1988), whereas 9.1 was obtained by

https://doi.org/10.1017/S0022112002008157 Published online by Cambridge University Press

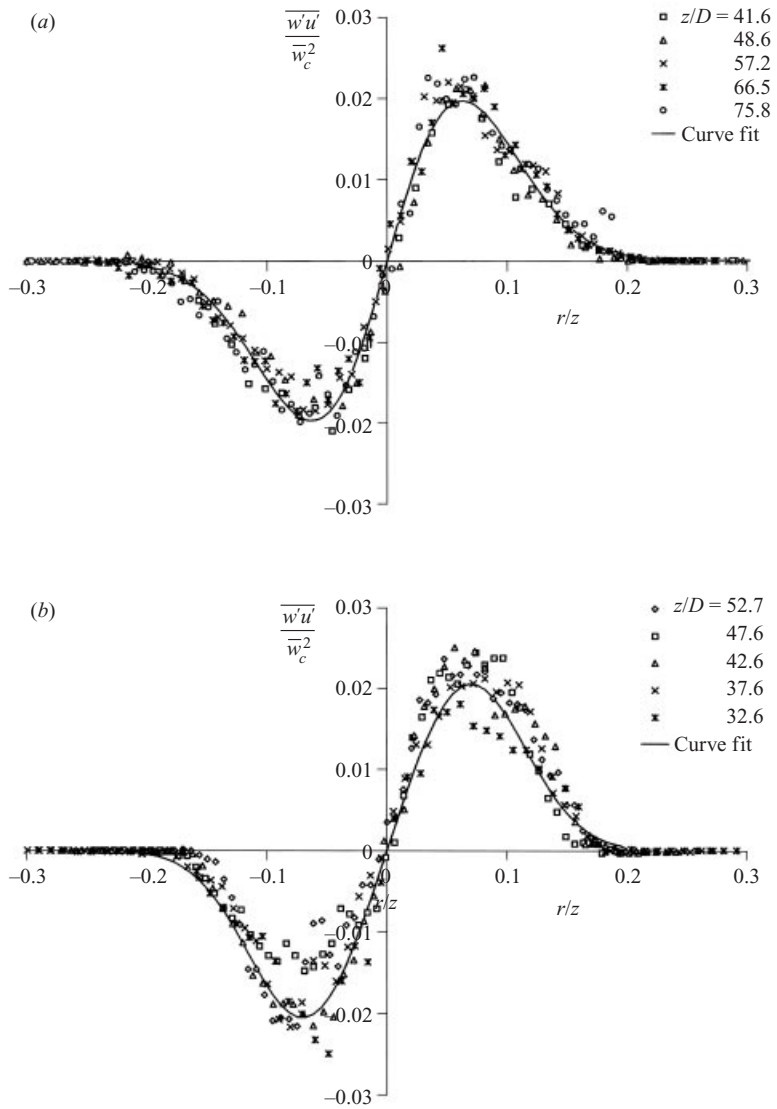


FIGURE 6. Cross-sectional variation of the normalized turbulent shear stress in (*a*) jets and (*b*) plumes.

George *et al.* (1977) and Fischer *et al.* (1979), and 9.4 by Shabbir & George (1994). It should be pointed out that the concentration decay constants of Papanicolaou & List are quoted from their earlier temperature measurements rather than their LIF results, since they realized that the LIF measurements overestimated the absolute time-averaged mean concentration. However, this should not significantly affect other quantities that were normalized by the corresponding centreline values.

The centreline decay of mean concentration in a buoyant jet is plotted in figure 7. Again the pure jet data are represented by their best-fit line (horizontal dotted line in the figure). The experimental data agree well with the asymptotic solutions, i.e. for $z/L_m < 0.6$ the flow is jet-like and for $z/L_m > 6$ the flow is plume-like. The smooth solid curve in the figure is computed from the second-order mass flux conservation

https://doi.org/10.1017/S0022112002008157 Published online by Cambridge University Press

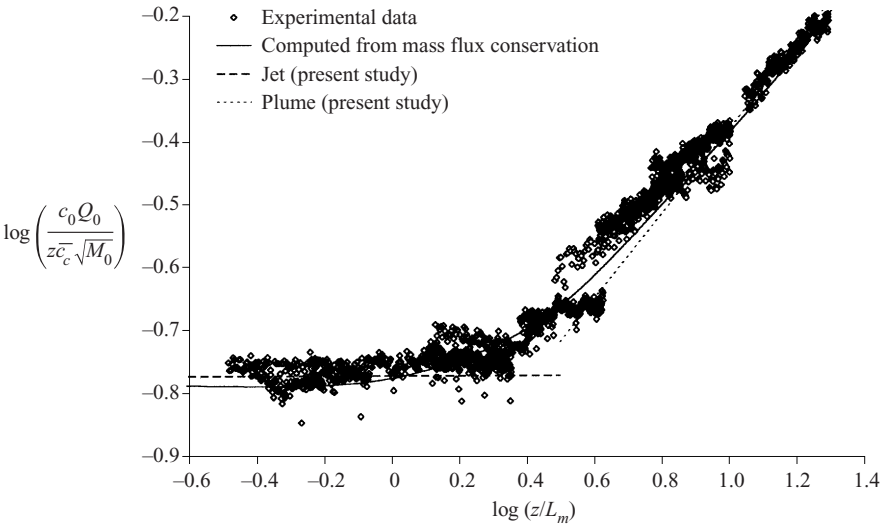


FIGURE 7. Centreline decay of the mean concentration in buoyant jets.

equation that will be introduced later. The experimental data collapse onto the theoretical curve quite well, indicating that the total mass flux is conserved within experimental errors.

The normalized cross-sectional profiles of mean concentration for jets and plumes follow the Gaussian distribution described by (15). The concentration spread rates (or dimensionless 1/e concentration widths) are determined to be: $\eta_{jc} = 0.129$ for jets and $\eta_{pc} = 0.109$ for plumes. Comparison with the literature (see tables 2 and 3) shows that the concentration width for jets obtained in the present study is in good agreement with others, while the concentration width for plumes is on the lower side. Unlike the velocity width, the concentration widths are quite different between jets and plumes, varying from 0.129 for jets to 0.109 for plumes. Similar observations were also reported in previous studies such as Papanicolaou & List (1988). The variation of concentration width during the transition from jet to plume is thus of interest. The experimental data are also plotted in figure 3. It can be seen that this variation is z/L_m-dependent.

The concentration fluctuations $\sqrt{\overline{c_c'^2}}/\overline{c_c}$ at the centreline were found to be about 22.4% for jets and 42% for plumes, in good agreement with past information. The cross-sectional profiles of concentration fluctuation for jets and plumes are shown in figures 8(*a*) and 8(*b*) respectively. It can be seen that the presence of buoyancy almost doubles the concentration fluctuations in plumes compared to jets. This is contrary to the buoyancy effect on turbulence velocity fluctuations discussed previously. Replaying the recorded DPIV vector maps and PLIF images showed that the flapping of the flow and the resulting intermittency are more pronounced in plumes than in jets. This observation was also noted by Papanicolaou & List (1989). The variation of centreline concentration fluctuations in a buoyant jet is plotted in figure 9. The figure clearly shows that the concentration fluctuation intensity is z/L_m dependent in the transitional region.

4.3. *Characteristics of turbulent mass transport*

Quantifying the turbulent mass transport in buoyant jets is one of the primary goals of this study. The cross-sectional variations of axial and radial turbulent mass transport

https://doi.org/10.1017/S0022112002008157 Published online by Cambridge University Press

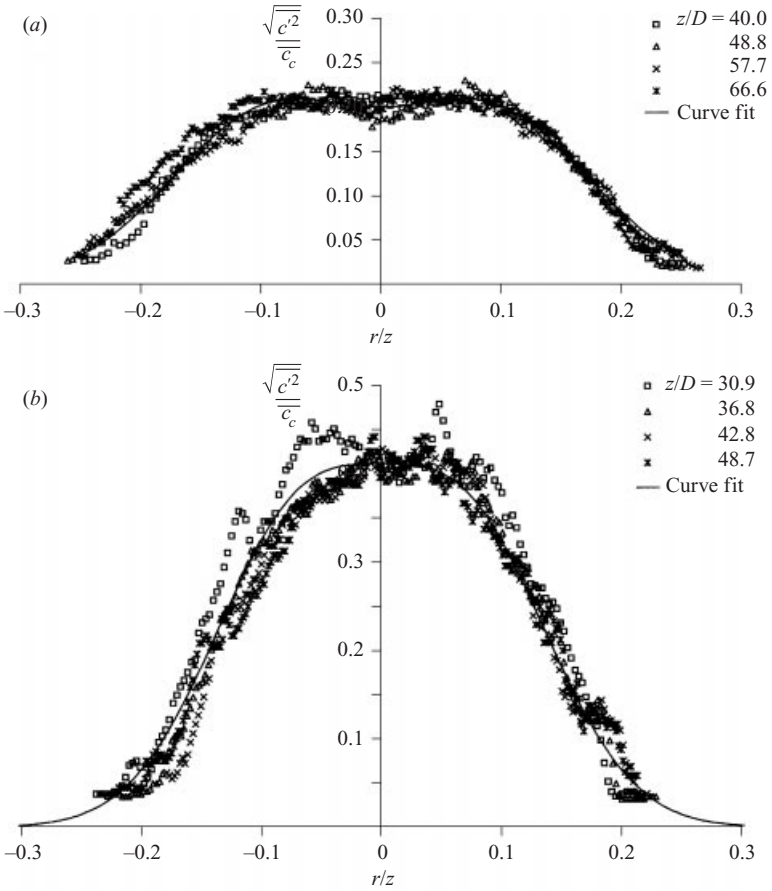


FIGURE 8. Cross-sectional variation of turbulent concentration fluctuation in (*a*) jets and (*b*) plumes.

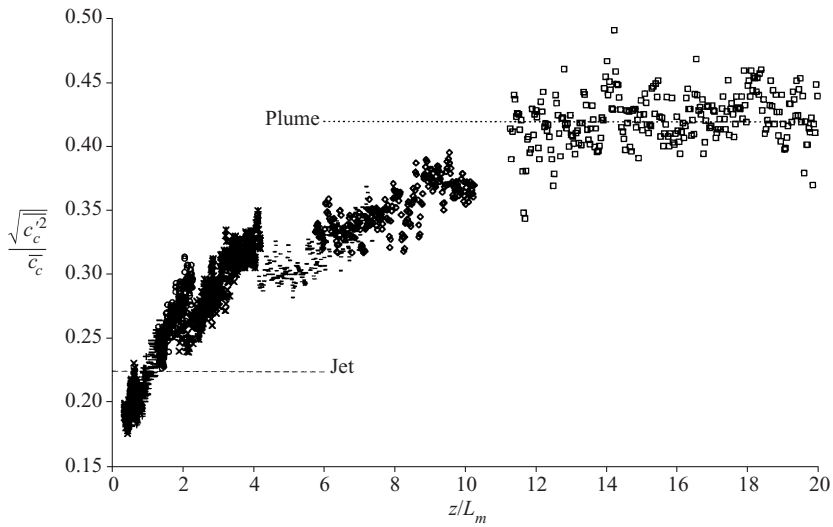


FIGURE 9. Variation of the centreline concentration fluctuation intensity with z/L_m in buoyant jets.

https://doi.org/10.1017/S0022112002008157 Published online by Cambridge University Press

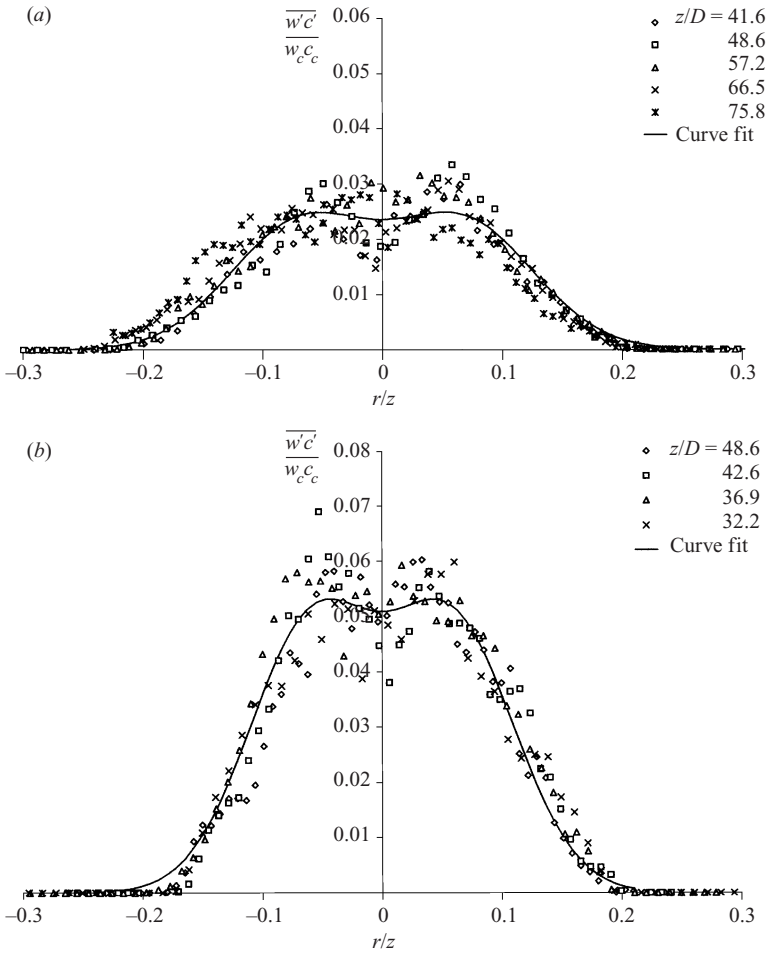


FIGURE 10. Cross-sectional variation of axial turbulent mass transport in (*a*) jets and (*b*) plumes.

in jets and plumes are plotted in figures 10 and 11 respectively. Figure 10(*a*) shows that the normalized axial turbulent mass transport along the jet centreline, $\overline{w_c'c_c'}/\overline{w_c c_c}$, has an average value of approximately 0.024. This value is within the range of past measurements of 0.03 by Antonia, Prabhu & Stephensen (1975), 0.021 by Chevray & Tutu (1978), and 0.020 by Papanicolaou & List (1988). The profiles of radial mass transport $\overline{u'c'}/\overline{w_c c_c}$ for jets (see figure 11*a*) collapse very well, with a peak value of approximately 0.018 located at $r/z \approx 0.7$, which is slightly higher than 0.015 by Papanicolaou & List (1988). More recently, Webster, Roberts & Ra'ad (1999) obtained similar turbulent mass transport results in a turbulent jet with combined digital particle tracking velocimetry (DPTV) and PLIF.

The centreline value of the normalized axial turbulent mass transport measured in plumes is about 0.05 (see figure 10*b*), in good agreement with 0.05 recorded by Papanicolaou & List (1988) and 0.056 by Shabbir & George (1994). Figure 10(*b*) also shows that the two off-centreline peaks are slightly higher than the centreline value. The radial mass transport in plumes has a peak value of about 0.031 at $r/z \approx 0.7$, as shown in figure 11(*b*). This is comparable to 0.028 by Shabbir & George (1994) but

https://doi.org/10.1017/S0022112002008157 Published online by Cambridge University Press

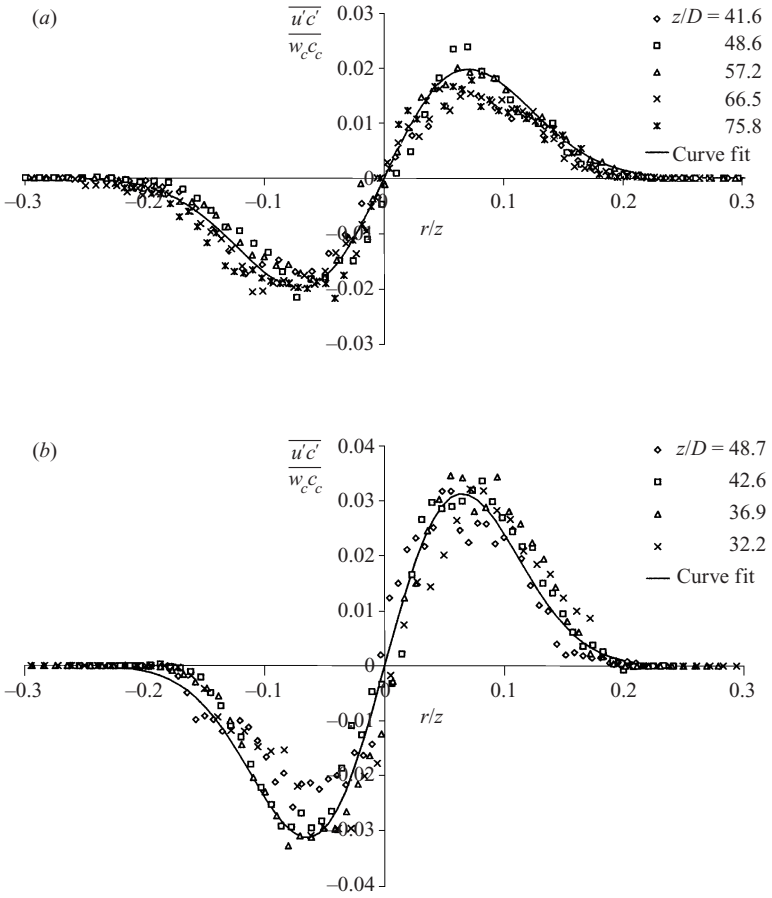


FIGURE 11. Cross-sectional variation of radial turbulent mass transport in (*a*) jets and (*b*) plumes.

higher than 0.020–0.025 reported by Papanicolaou & List (1988). Comparison between the jet and plume results shows that the axial and radial turbulent mass transports in plumes are almost twice those in jets, which could be a direct consequence of the nearly double concentration fluctuation in plumes.

4.4. *Curve-fitting results of turbulent characteristics in jets and plumes*

An important advantage of combined DPIV and PLIF is that an adequate two-dimensional planar distribution for velocity and concentration fields can be acquired within a short duration. This is in contrast to using a point-based instrument that typically requires an experimentation time in the order of hours to resolve the cross-sectional distribution of the physical quantities. Unexpected changes in the experimental conditions may occur in such a long time (e.g. positioning error introduced by the traversing system, ambient temperature variation, self-contamination, inconsistency of the exit conditions, etc.). The advantage of the current approach could explain the generally less scatter in the data reported here. The twin $1\text{k} \times 1\text{k}$ resolution digital cameras provide very high spatial data density and thus are also potentially more accurate in identifying the cross-sectional profiles as well as determining the flux-related quantities.

https://doi.org/10.1017/S0022112002008157 Published online by Cambridge University Press

	Pure axisymmetric jet			Pure axisymmetric plume		
	A	k_g	η_0	A	k_g	η_0
$\sqrt{\overline{w'^2}}/\overline{w_c}$	0.2151	83.46	0.07318	0.2361	113.4	0.07222
$\sqrt{\overline{u'^2}}/\overline{w_c}$	0.1513	75.49	0.07672	0.1533	90.51	0.07578
$\overline{w'u'}/\overline{w_c}^2$	0.06110	129.4	0.01691	0.02084	224.4	0.06815
$\sqrt{\overline{c'^2}}/\overline{c_c}$	0.1900	73.15	0.09360	0.3323	97.12	0.07023
$\overline{w'c'}/\overline{w_c c_c}$	0.02276	143.1	0.06788	0.04818	183.6	0.05893
$\overline{u'c'}/\overline{w_c c_c}$	0.02381	129.2	0.05392	0.03607	163.9	0.05199

TABLE 4. Curve-fitting results for turbulence quantities.

The turbulence data are fitted with empirical curves in the forms

$$f(\eta) = A\{\exp[-k_g(\eta-\eta_0)^2] + \exp[-k_g(\eta+\eta_0)^2]\} \tag{33}$$

for the quantities with a symmetric cross-sectional distribution and

$$f(\eta) = A\{\exp[-k_g(\eta-\eta_0)^2] - \exp[-k_g(\eta+\eta_0)^2]\} \tag{34}$$

for those with an antisymmetric cross-sectional distribution, where $\eta = r/z$. The constants A, k_g and η_0 are determined using the least-square method. The results are tabulated in table 4.

4.5. *Data verification using theoretical criteria*

Using the combined DPIV and PLIF approach, an enormous amount of planar information was captured with high spatial density. This enables a close examination of the data quality with the available theoretical criteria. It has been shown that the cross-sectional profiles in the present study satisfy the symmetry or antisymmetry requirement very well. Additional verification includes the closure check on momentum and mass flux conservation, turbulent shear stress and radial turbulent mass transport. The verification is necessary and important as the experimental data will be used as the basis for the proposed second-order integral model.

4.5.1. *Momentum and mass flux conservation*

Based on the curve-fitting results reported previously, it can be computed that

$$k_{jM} = 1 + \frac{M_{TP}}{M_M} = 1.10, \tag{35}$$

$$k_{pM} = 1 + \frac{M_{TP}}{M_M} = 1.10, \tag{36}$$

$$k_{jH} = 1 + \frac{H_T}{H_M} = 1.076, \tag{37}$$

$$k_{pH} = 1 + \frac{H_T}{H_M} = 1.15. \tag{38}$$

Equations (35) and (36) show that the momentum flux contributed by the turbulence and streamwise pressure gradient is about 10% of the mean momentum flux in both jets and plumes. The same percentage in jets and plumes is a result of the similarity in the turbulence velocity field as illustrated previously. As a comparison, a value of

https://doi.org/10.1017/S0022112002008157 Published online by Cambridge University Press

4.6% for plumes was reported by Shabbir & George (1994). The difference between the current study and Shabbir & George (1994) is mainly due to the difference in η_{pw}. Papanicolaou & List (1988) reported a percentage of 15% for both jets and plumes without taking into account the negative contribution from the streamwise pressure gradient. On the other hand, (37) and (38) indicate that the amount of turbulent mass flux is very different for jets and plumes. It takes the values of 7.6% and 15% of the mean mass flux in jets and plumes respectively. These percentages are certainly not trivial and should be accounted for in the integral models.

In a jet, the total momentum flux is conserved and equal to the momentum flux introduced at the source. This imposes a constraint on the experimental constants:

$$k_{jM}k_{jw}^2\eta_{jw}^2 = 0.5. \tag{39}$$

Substituting the measured constants in the above equation yields a momentum conservation error of 3% in the jet experiments. For plumes, (6) dictates

$$\tfrac{2}{3}k_{pM}k_{pw}^2\eta_{pw}^2 = k_{pc}\eta_{pc}^2. \tag{40}$$

The plume results from the present study satisfy the above equation with an error of 2%.

The total mass (buoyancy) flux should be conserved and equal to the source flux in both jets and plumes. Thus, the following constraints apply:

$$k_{jH}\frac{k_{jw}k_{jc}\eta_{jw}^2\eta_{jc}^2}{\eta_{jw}^2+\eta_{jc}^2} = 0.25, \tag{41}$$

$$k_{pH}\frac{\pi k_{pw}k_{pc}\eta_{pw}^2\eta_{pc}^2}{\eta_{pw}^2+\eta_{pc}^2} = 1. \tag{42}$$

Substituting the jet and plume results into the above equations shows that 98% and 96% of the source mass flux is conserved in the jet and plume experiments respectively. The closure errors are very small, implying good data accuracy.

4.5.2. *Radial mass and momentum transport*

Integrating (3) and (2) across the cross-sectional area of the buoyant jet from 0 to r with the help of (1) yields

$$\frac{\partial}{\partial z}\int_0^r (\overline{wc}+\overline{w'c'})\,r\,\mathrm{d}r + (\overline{uc}+\overline{u'c'})r = 0, \tag{43}$$

$$\frac{\partial}{\partial z}\int_0^r (\bar{w}^2+\overline{w'^2}-\overline{u'^2})\,r\,\mathrm{d}r + (\overline{wu}+\overline{w'u'})r - \int_0^r g\frac{\overline{\Delta\rho}}{\rho_a}r\,\mathrm{d}r = 0. \tag{44}$$

The above equations reflect the balance of the axial and radial transport of momentum and mass in a control volume centred at the axis of the buoyant jet with a radius r, as sketched in figure 12. Equation (43) shows that in the control volume, the axial rate of change of the total axial mass flux is balanced by the total radial mass flux, while (44) indicates that the axial rate of change of the total axial momentum flux is balanced by the radial mean and turbulent flux of the axial momentum, the buoyancy force and the streamwise pressure gradient. The variation of individual terms in the two equations in both jets and plumes are plotted in figures 13 and 14. The 'error' terms in the figures represent the residue of the left-hand side of the above equations.

Figures 13(a) and 13(b) show that the rate of loss of axial turbulent mass flux is very

https://doi.org/10.1017/S0022112002008157 Published online by Cambridge University Press

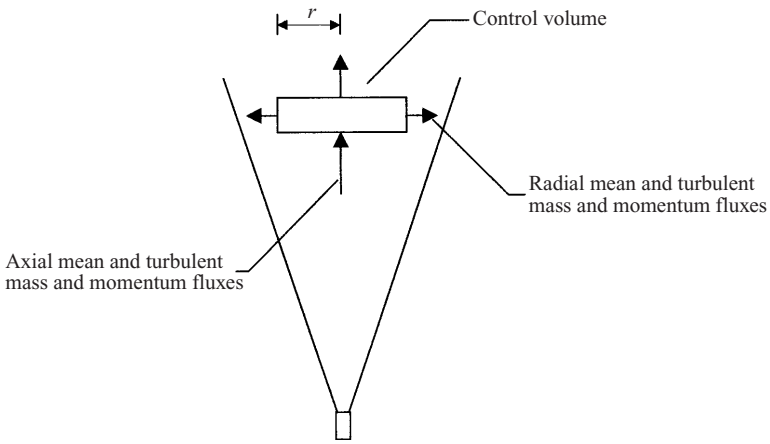


FIGURE 12. Sketch showing the balance of the axial and radial mass and momentum transports in a control volume.

small compared with that of axial mean mass flux. The loss of total axial mass flux in the control volume is balanced mainly by the outward radial turbulent mass flux. This implies that the tracer mass is transported laterally through turbulent diffusion. A distinct difference between the two figures is that in jets, the radial mean mass flux is positive (outward) when $r/z < 0.12$ and becomes negative (inward) beyond this range, whereas in plumes, the critical point is much closer to the centreline, at $r/z \approx 0.06$. As a result, the inward radial mean mass flux is more pronounced in plumes than in jets, and the lateral transport of tracer mass depends more on the radial turbulent diffusion in plumes. It should be noted that when the radial mean mass flux becomes negative (inward), the tracer mass can still be transported outwards through turbulent diffusion. All terms in (43) become zero when $r/z \to \infty$, implying that the total axial mass flux is conserved. Equation (43) provides a way to theoretically compute the radial turbulent mass transport and therefore constitutes a criterion to check the experimental results. The small magnitude of the error terms in figure 13 confirms the quality of the measured radial turbulent mass transport in this study. The errors are not only due to the possible underestimation of the radial turbulent mass transport but also the inaccuracy in quantifying other quantities as well as the curve-fitting procedures. Furthermore, compared with the mean axial mass transport, the turbulent mass transports in both the axial and radial directions are of second order. Hence, the error terms in figure 13 are indeed very small. In terms of measurement techniques, there is little difference between the radial and axial turbulent mass transport. This would imply that the axial turbulent mass transport determined in the present study is also of high quality.

Figure 14(a) shows that in jets the loss of total axial momentum flux along the axial direction in the control volume is balanced mainly by the outward radial turbulent axial-momentum flux ($r\overline{w'u'}$), i.e. the axial momentum is transported laterally mainly through turbulent diffusion. Beyond $r/z \approx 0.12$, the radial mean axial-momentum flux ($r\overline{w}\overline{u}$) becomes negative and the axial momentum is transported laterally by overcoming this inward advective flux. Again all terms in the figure approach zero when $r/z \to \infty$, implying that the total axial momentum flux including the contribution of streamwise pressure gradient is conserved. The lateral transport of axial

https://doi.org/10.1017/S0022112002008157 Published online by Cambridge University Press

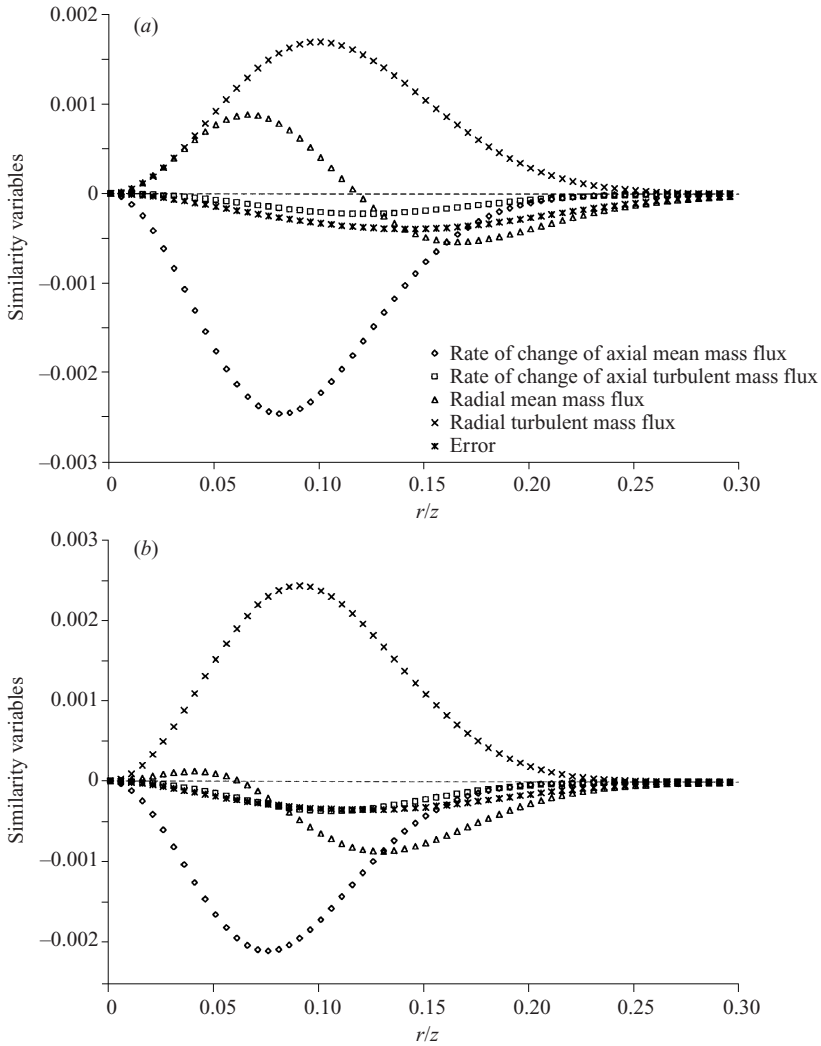


FIGURE 13. Balance of the axial and radial mass transports in a control volume in (*a*) jets and (*b*) plumes.

momentum relies more on the radial turbulent diffusion in plumes (see figure 14(*b*)). When $r/z > 0.06$, the transport is achieved by overcoming the inward advection.

Unlike the jet case, the lateral transport of axial momentum in plumes does not necessarily result in a loss of it in the control volume. In fact, beyond $r/z \approx 0.065$, the axial momentum contained in the control volume starts to increase. This is because the buoyancy force produces much of the additional momentum. When $r/z \to \infty$, i.e. the control volume becomes the entire cross-sectional area of the plume, the radial mean and turbulent axial-momentum fluxes approach zero. Therefore the rate of increase of total axial momentum flux including the contribution of steamwise pressure gradient is equal to the buoyancy force. This has already been illustrated in (6). Equation (44) provides an approach to theoretically compute the radial turbulent axial-momentum transport, i.e. the turbulent shear stress, and therefore constitutes a

https://doi.org/10.1017/S0022112002008157 Published online by Cambridge University Press

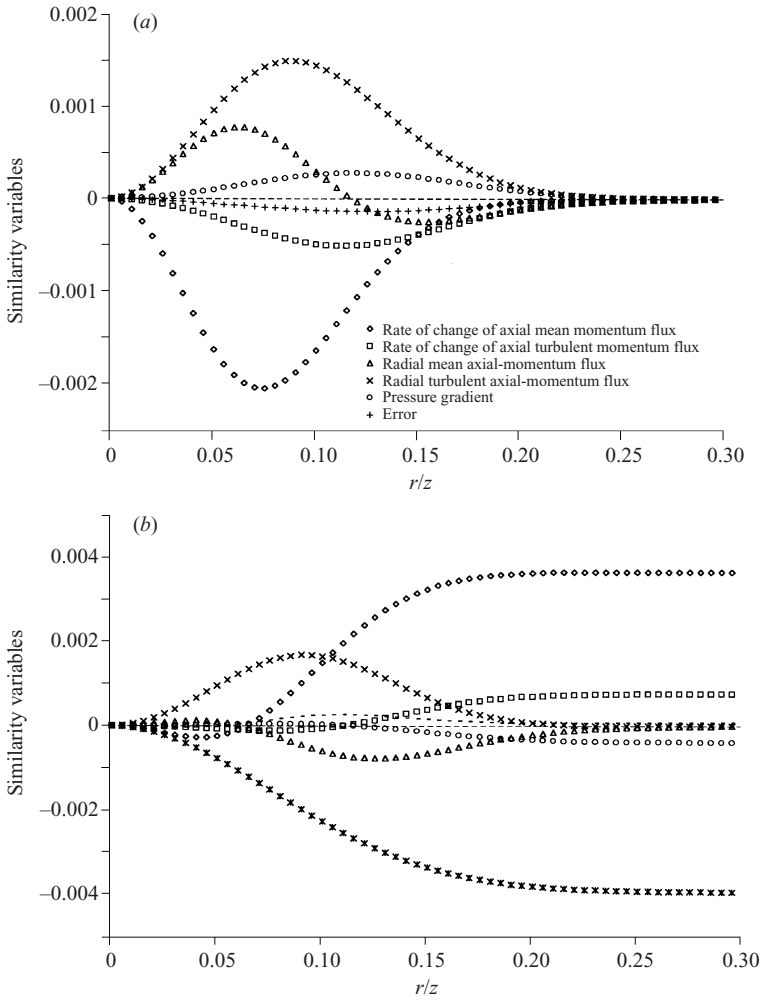


FIGURE 14. Balance of the axial and radial axial-momentum transports in a control volume in (*a*) jets and (*b*) plumes.

criterion to check the experimental results. The small magnitude of the error terms in figure 14 confirms the quality of the measured shear stresses.

4.6. *Experimental results concerning the second-order integral model*

4.6.1. *Relationship between local Richardson number R and z/L_m*

As shown previously, for a vertical buoyant jet, z/L_m is an important parameter to characterize the flow transition from jet-like to plume-like. However, this transition also occurs in other situations such as horizontal buoyant jets or buoyant jets in a cross-flow where z/L_m is not applicable. Since the conclusions (e.g. the variations of shear entrainment coefficient, concentration spread rate and H_T/H_M during the transition) drawn from the vertical buoyant jet case may also be applicable to other situations, it is preferable to use the more commonly used local parameters such as the local Richardson number R rather than z/L_m to quantify the transitional variations

https://doi.org/10.1017/S0022112002008157 Published online by Cambridge University Press

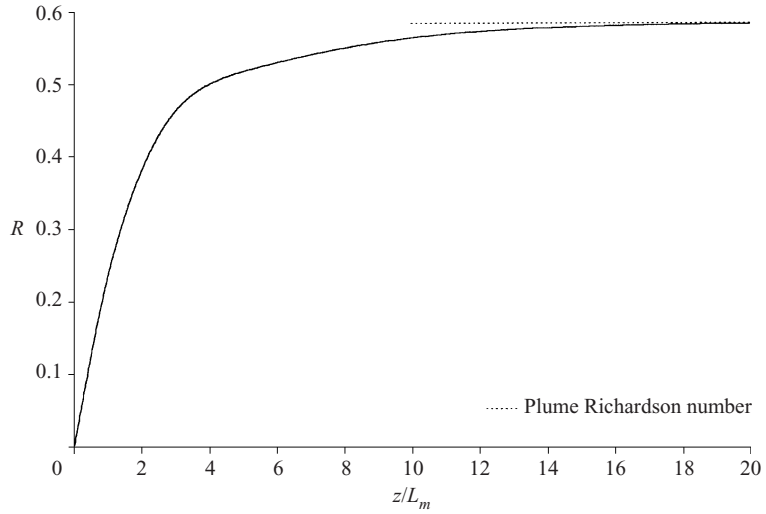


FIGURE 15. Variation of the local Richardson number with z/L_m in buoyant jets.

of the flow characteristics. We will therefore derive the relationship between R and z/L_m as follows.

The present study shows that k_M and η_w are nearly constant throughout the transition, i.e. $k_M = k_{jM} = k_{pM} = 1.1$ and $\eta_w = \eta_{jw} = \eta_{pw} = 0.105$. Also, in a non-stratified environment, we have $B = B_0$. Together with the empirical curve fitting equations (27), (28) and (29) for $\overline{w_c}$, the relationship between R and z/L_m can be established based on (22) as

$$R = 2^{5/4}\pi^{-1/4}k_M^{-5/4}\eta_w^{-1/2}10^{3g(\xi)/2}\frac{z}{L_m}, \tag{45}$$

The above equation shows that the local R is directly related to z/L_m. Their relationship is plotted in figure 15. In pure jets, both z/L_m and R are zero. In the jet-like region, R increases linearly with z/L_m. The relationship becomes nonlinear in the transitional region and subsequently R becomes constant in the plume-like region. The constant is called the plume Richardson number, R_p, which is determined to be 0.584 in the experiments.

4.6.2. *Variation of entrainment coefficient*

As mentioned previously, the entrainment coefficient in a buoyant jet can be modelled by (20) or (21). However, there have been few experimental evaluations of the prediction accuracy of these two commonly used formulations in the transitional region from jet-like to plume-like. In this study, a large amount of experimental data was obtained in the transitional region, and the empirical curve fit result for the centreline mean axial velocity is very close to the experimental data (see figure 2). We are thus able to give an evaluation of the two formulations.

With the help of the centreline axial velocity curve fit equations (27), (28) and (29), the variation of α with z/L_m can be derived based on the entrainment assumption equation (19) as

$$\alpha = \frac{\eta_w}{2}\left[1 - \frac{\mathrm{d}g(\xi)}{\mathrm{d}\xi}\right], \tag{46}$$

with $\alpha_j = \eta_{jw}/2 = 0.0525$ for jets and $\alpha_p = 5\eta_{pw}/6 = 0.0875$ for plumes. The

https://doi.org/10.1017/S0022112002008157 Published online by Cambridge University Press

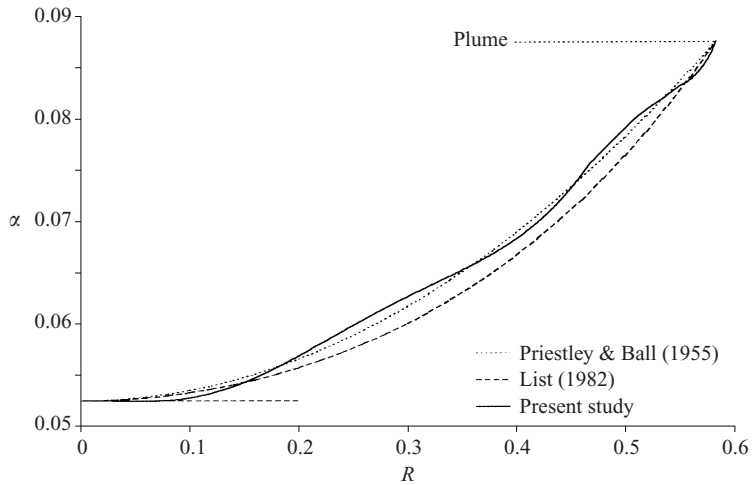


FIGURE 16. Variation of the entrainment coefficient with the local Richardson number in buoyant jets.

relationship between α and R can then be determined implicitly by (45) and (46). The results are shown in figure 16. It can be observed that the experimental curve is not as smooth as expected. This is caused by the derivative operation on the empirical curve fit obtained on a log-log graph as shown in figure 2. Despite the small undulation, it can be seen that both (20) and (21) are in good agreement with the experimental curve, with the former appears to be more realistic. We will thus adopt (20) for the second-order integral model.

4.6.3. *Variation of concentration-to-velocity width ratio* λ

As shown previously in figure 3, while the velocity spread rate remains nearly constant during the transition from jet to plume, the concentration spread rate varies. This results in a varying λ. Although the variation of concentration spread rate is relatively small, it would lead to an error of up to 15% in the conservation of mass flux if ignored. Therefore, modelling this variation is very important to achieve second-order closure. In the existing integral models, the width ratio λ is generally assumed to be a constant (e.g. Fischer *et al.* 1979; Wood *et al.* 1993) and usually the value of the plume width ratio λ_p is adopted due to the fact that any buoyant jet will eventually become plume-like. A previous study by Noutsopoulos & Yannopoulos (1987) did not assume a constant λ in their integral model. Instead, they assumed that $\eta_w(1+\lambda^2) =$ constant. Together with a semi-empirical z/L_m-dependent expression of the velocity spread rate η_w, they were able to obtain an analytical solution of the vertical buoyant jet. Their results led to a nearly constant concentration spread rate and a z/L_m-dependent velocity spread rate with 20% variation from jet to plume, which differs significantly to the observations here.

The variation of λ with R can be computed based on figure 3 and (45), and the results are plotted in figure 17. The figure shows that λ varies from $\lambda_j = 1.23$ to $\lambda_p = 1.04$ during the transition. As a comparison, $\lambda_j = 1.21$ and $\lambda_p = 1.06$ were reported by Papanicolaou & List (1988). To provide a simple empirical quantitative description of the relationship between λ and R, the following form is used for the

https://doi.org/10.1017/S0022112002008157 Published online by Cambridge University Press

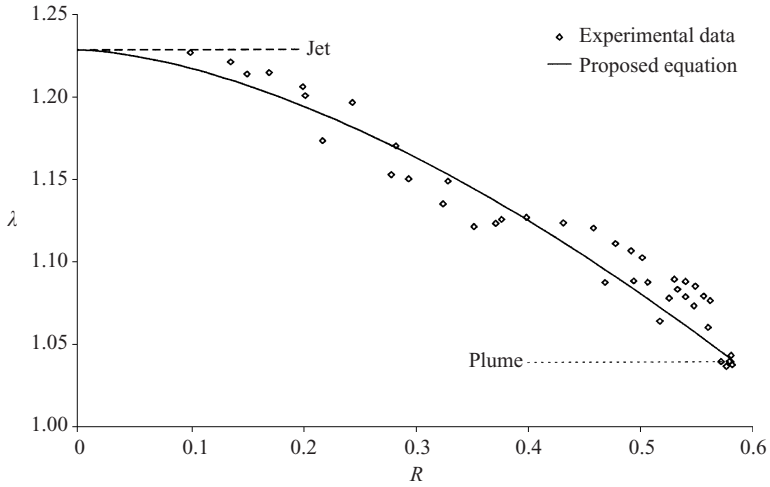


FIGURE 17. Variation of the concentration-to-velocity width ratio with the local Richardson number in buoyant jets.

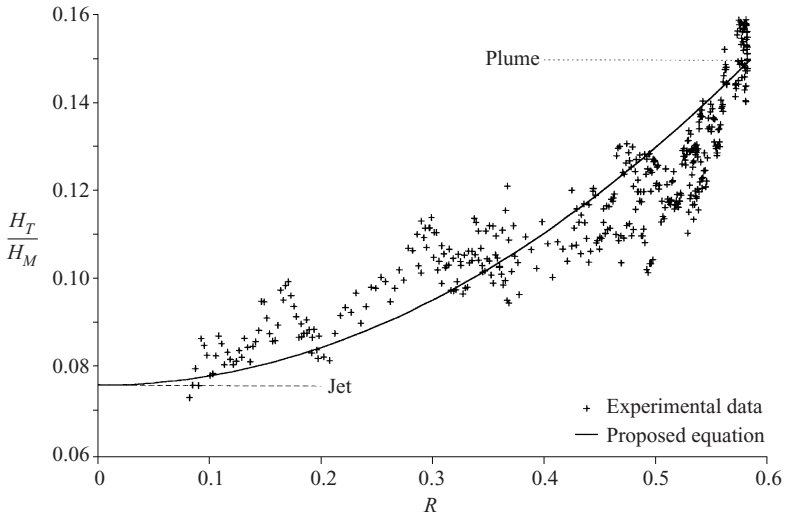


FIGURE 18. Variation of the ratio of the axial turbulent mass flux to the axial mean mass flux with the local Richardson number in buoyant jets.

interpolation between λ_j and λ_p:

$$\lambda = \lambda_j - (\lambda_j - \lambda_p)\left(\frac{R}{R_p}\right)^{\sigma}, \tag{47}$$

where $\sigma = 1.5$ fits reasonably well the experimental data. Equation (47) with $\sigma = 1.5$, $\lambda_j = 1.23$ and $\lambda_p = 1.04$ is thus proposed for the relationship between λ and R.

4.6.4. *Turbulent mass flux*

The cross-sectional profiles of axial and radial turbulent mass transport of buoyant jets have similar shapes to those of jets (see figures 10*a* and 11*a*) and plumes (see figures 10*b* and 11*b*) but with the magnitudes varying in between. Of particular interest

https://doi.org/10.1017/S0022112002008157 Published online by Cambridge University Press

here is the variation of the ratio of axial turbulent mass flux to axial mean mass flux, H_T/H_M, because the ratio is important for the total mass flux conservation. The cross-sectional profiles of axial turbulent mass transport in the zone of flow establishment are integrated individually and the ratio, H_T/H_M, is plotted with respect to R in figure 18. Despite the scatter among the experimental data, the trend of the variation is reasonably well captured. Again, to model this variation, a simple empirical interpolation equation can be used in the form

$$\frac{H_T}{H_M} = \left(\frac{H_T}{H_M}\right)_j - \left[\left(\frac{H_T}{H_M}\right)_j - \left(\frac{H_T}{H_M}\right)_p\right]\left(\frac{R}{R_p}\right)^{\sigma}, \tag{48}$$

where $\sigma = 2$ appears to fit reasonably well the experimental data. Equation (48) with $\sigma = 2$, $(H_T/H_M)_j = 7.6\%$ and $(H_T/H_M)_p = 15\%$ are thus proposed for the relationship between H_T/H_M and R. The above equation can be rewritten in terms of the ratio of total mass flux to mean mass flux, k_H, as

$$k_H = k_{jH} - (k_{jH} - k_{pH})\left(\frac{R}{R_p}\right)^{\sigma}, \tag{49}$$

where $\sigma = 2$, $k_{jH} = 1.076$ and $k_{pH} = 1.15$.

5. Second-order integral model of buoyant jets

Based on the above findings, a second-order integral model can finally be formulated for a vertical buoyant jet discharging into a stagnant uniform ambient. The model covers the full transition from jet-like to plume-like. The balance equations for mass and momentum are computed to second-order, which means the turbulent momentum and mass fluxes as well as the variation of concentration-to-velocity width ratio during the transition are all taken into account. The proposed model can be modified to suit other situations of buoyant jets to achieve second-order closure of both total momentum and mass fluxes. The individual equations for the model have already been put forward previously. They are summarized as follows:

continuity:

$$\frac{\mathrm{d}Q}{\mathrm{d}z} = \frac{\mathrm{d}}{\mathrm{d}z}(\pi\bar{w}_c\eta_w^2 z^2) = 2\pi\alpha\eta_w z\bar{w}_c, \tag{50}$$

momentum:

$$\frac{\mathrm{d}M}{\mathrm{d}z} = \frac{\mathrm{d}}{\mathrm{d}z}\left(k_M\frac{\pi}{2}\bar{w}_c^2\eta_w^2 z^2\right) = \pi\overline{\Delta_c}\lambda^2\eta_w^2 z^2, \tag{51}$$

buoyancy flux conservation:

$$\frac{\mathrm{d}B}{\mathrm{d}z} = \frac{\mathrm{d}}{\mathrm{d}z}\left(k_H\frac{\lambda^2}{1+\lambda^2}\pi\overline{w_c\Delta_c}\eta_w^2 z^2\right) = 0, \tag{52}$$

entrainment coefficient:

$$\alpha = \alpha_j - (\alpha_j - \alpha_p)\left(\frac{R}{R_p}\right)^2, \tag{53}$$

concentration-to-velocity width ratio:

$$\lambda = \lambda_j - (\lambda_j - \lambda_p)\left(\frac{R}{R_p}\right)^{3/2}, \tag{54}$$

https://doi.org/10.1017/S0022112002008157 Published online by Cambridge University Press

Ratio of the total mass flux to the mean:

$$k_H = k_{jH} - (k_{jH} - k_{pH}) \left(\frac{R}{R_p} \right)^2, \tag{55}$$

where

$$R = 2^{5/4} \pi^{1/4} k_H^{1/2} k_M^{-5/4} \overline{w_c}^{-1} \overline{\Delta_c}^{1/2} \lambda \eta_2^{3/2} (\eta_c^2 + \eta_w^2)^{-1/2} z^{1/2}. \tag{56}$$

All constants involved in the above set of equations have already been calibrated: $\alpha_j = 0.0525$, $\alpha_p = 0.0875$, $\lambda_j = 1.23$, $\lambda_p = 1.04$, $k_{jH} = 1.076$, $k_{pH} = 1.15$, $k_M = 1.1$, $R_p = 0.584$. After substituting (56) into (53), (54) and (55), the remaining unknowns are α, λ, k_H, η_w, $\overline{w_c}$ and $\overline{\Delta_c}$. With the six equations (50)–(55), the six unknowns can be readily solved using numerical methods. The initial conditions can be given at the end of the zone of flow establishment (ZFE) using models such as Abraham (1963), Lee, Jirka & Harleman (1974) and Lee (1980).

6. Summary

Simultaneous measurements of turbulent velocity and concentration fields of round vertical pure jets and buoyant jets have been reported using a combined DPIV and PLIF approach. A unique feature with the combination of the two experimental techniques is that the covariance of the instantaneous velocity and concentration fields is readily revealed. This provides more insight into the mixing processes than if the two techniques are individually performed. Comprehensive self-checks on the symmetry, mass and momentum conservation, turbulent shear stress and radial turbulent mass transport are examined based on the large amount of planar information obtained. The validation shows that good data quality was achieved.

The jet and plume results are mostly in agreement with those reported previously in the literature. The differences between the plume data obtained in the present study and those based on temperature measurements in air are however noted. In the fully developed region, the buoyancy has no apparent effect on turbulence velocity fluctuations. In contrast, the concentration fluctuations are significantly intensified by the buoyancy force. This is accompanied by the increased turbulent mass transport.

The radial mass transport and turbulent shear stress are found to be of first-order importance in the turbulence modelling of buoyant jets. Nevertheless, the integral models avoid modelling these terms by integrating the governing differential equation over the cross-sectional area. Although the axial turbulent mass and momentum fluxes are of second-order compared with the axial advective fluxes, they are not negligibly small and should be incorporated for better prediction.

The measurements in the transitional region detailed the evolution from jet-like to plume-like and provided the experimental basis for the integral modelling effort. It has been shown that the variations of axial turbulent mass flux and concentration-to-velocity width ratio can also be appropriately modelled as functions of the local Richardson number, while the momentum flux contributed by the turbulence and streamwise pressure gradient can be taken into account as a fixed percentage of the mean. Other than the vertical buoyant jet in stagnant fluid, the proposed second-order integral model can be modified to suit more complicated flow configurations. This will be further explored in future studies.

Funding for this study provided by the Academic Research Fund (11/96) of the Nanyang Technological University is gratefully acknowledged.

https://doi.org/10.1017/S0022112002008157 Published online by Cambridge University Press

REFERENCES

Abraham, G. 1963 *Jet Diffusion in Stagnant Ambient Fluid*. Delft Hydraulics Laboratory, Publication 29.

Antonia, R. A., Prabhu, A. & Stephenson, S. E. 1975. Conditionally sampled measurements in a heated turbulent jet. *J. Fluid Mech.* **72**, 455–480.

Baker, C. B. 1980 An analysis of the turbulent buoyant jet. PhD Thesis, Pennsylvania State University, USA.

Berlman, I. B. 1971 *Handbook of Fluorescence Spectra of Aromatic Molecules*, 2nd Edn. Academic.

Capp, S. P. 1983 Experimental investigation of the buoyant axisymmetric jet. PhD Thesis, University at Buffalo, State University of New York, USA.

Chen, J. C. & Rodi, W. 1980 *Turbulent Buoyant Jets – A Review of Experimental Data*. Pergamon.

Chevray, R. & Tutu, N. K. 1978 Intermittency and preferential transport of heat in a round jet. *J. Fluid Mech.* **88**, 133–160.

Corrsin, S. & Uberoi, M. S. 1950 Further experiments on the flow and heat transfer in a heated turbulent air jet. *NACA Rep.* 998.

Dahm, W. J. A. & Dimotakis, P. E. 1990 Mixing at large Schmidt number in the self-similar far field of turbulent jets. *J. Fluid Mech.* **217**, 299–330.

Fischer, H. B., List, E. J., Imberger, J. & Brooks, N. H. 1979 *Mixing in Inland and Coastal Waters*. Academic.

George, W. K. 1990 Governing equations, experiments and the experimentalist. *Expl Thermal Fluid Sci.* **3**, 557–566.

George, W. K., Alpert, R. L. & Tamanini, F. 1977 Turbulence measurements in an axisymmetric buoyant plume. *Intl J. Heat Mass Transfer* **20**, 1145–1154.

Hussein, H. J., Capp, S. P. & George, W. K. 1994 Velocity measurements in a high-Reynolds-number, momentum-conserving, axisymmetric, turbulent jet. *J. Fluid Mech.* **258**, 31–75.

Jirka, G. H. & Harleman, D. R. F. 1979 Stability and mixing of vertical plane jets in a confined depth. *J. Fluid Mech.* **94**, 275–304.

Jones, D. G. & Baddour, R. E. 1991 Vertical thermal-buoyant jets. *J. Hydraul. Res.* **29**(5), 601–613.

Law, A. W.-K. & Wang, H. 2000 Measurements of mixing processes using combined DPIV and PLIF. *Expl Thermal Fluid Sci.* **22**, 213–229.

Lee, J. H. W. 1980 Stability and mixing of a round buoyant discharge in shallow water. *2nd Intl Symp. on Stratified Flows, Trondheim*, Vol. 2, pp. 881–897.

Lee, J. H. W., Jirka, G. H. & Harleman, D. R. F. 1974 Stability and mixing of a vertical round buoyant jet in shallow water. *MIT Rep. 185*. Ralph M. Parsons Lab.

List, E. J. 1982 Mechanics of turbulent buoyant jets and plumes. *Turbulent Buoyant Jets and Plumes* (ed. W. Rodi), pp. 1–68. Pergamon.

List, E. J. & Imberger, J. 1973 Turbulent entrainment in buoyant jets and plumes. *J. Hydraul. Div. ASCE* **99**(9), 1461–1474.

Mei, R. 1996 Velocity fidelity of flow tracer particles. *Exps. Fluids* **22**, 1–13.

Morton, B. R., Taylor, G. I. & Turner, J. S. 1956 Turbulent gravitational convection from maintained and instantaneous sources. *Proc. R. Soc. Lond.* A **234**, 1–23.

Noutsopoulos, G. & Yannopoulos, P. 1987 The round vertical turbulent buoyant jet. *J. Hydraul. Res.* **25**(1), 481–501.

Panchapakesan, N. R. & Lumley, J. L. 1993*a* Turbulent measurements in axisymmetric jets of air and helium. Part 1. Air jet. *J. Fluid Mech.* **246**, 197–223.

Panchapakesan, N. R. & Lumley, J. L. 1993*b* Turbulent measurements in axisymmetric jets of air and helium. Part 2. Helium jet. *J. Fluid Mech.* **246**, 225–247.

Papanicolaou, P. N. 1984 Mass and momentum transport in a turbulent buoyant vertical axisymmetric jet. PhD Thesis, California Institute of Technology, USA.

Papanicolaou, P. N. & List, E. J. 1988 Investigations of round vertical turbulent buoyant jets. *J. Fluid Mech.* **195**, 341–391.

Papantoniou, D. & List, E. J. 1989 Large-scale structure in the far field of buoyant jets. *J. Fluid Mech.* **209**, 151–190.

Peterson, J. & Bayazitoglu, Y. 1992 Measurements of velocity and turbulence in vertical axisymmetric isothermal and buoyant jets. *J. Heat Transfer* **114**, 135–142.

https://doi.org/10.1017/S0022112002008157 Published online by Cambridge University Press

Priestley, C. H. B. & Ball, F. K. 1955 Continuous convection from an isolated source of heat. *Q. J. R. Met. Soc.* **81**, 144–157.

Rouse, H., Yih, C. S. & Humphreys, H. W. 1952 Gravitational convection from a boundary source. *Tellus* **4**, 201–210.

Seif, A. A. 1981 Higher order closure model for turbulent jets. PhD Thesis, University at Buffalo, State University of New York, USA.

Shabbir, A. & George, W. K. 1994 Experiments on a round turbulent buoyant plume. *J. Fluid Mech.* **275**, 1–32.

Wang, H. 2000 Investigations of buoyant jet discharges using digital particle image velocimetry (DPIV) and planar laser induced fluorescence (PLIF). PhD Thesis, Nanyang Technological University, Singapore.

Webster, D. R., Roberts, P. J. W. & Ra'ad, L. 1999 Simultaneous DPTV/PLIF measurements of a turbulent jet. *3rd Intl Workshop on PIV, Santa Barbara, USA*, pp. 599–605.

Wood, I. R., Bell, R. G. & Wilkinson, D. L. 1993 *Ocean Disposal of Wastewater*. World Scientific.

Wygnanski, I. & Fiedler, H. 1969 Some measurements in the self-preserving jet. *J. Fluid Mech.* **38**, 577–612.

https://doi.org/10.1017/S0022112002008157 Published online by Cambridge University Press